Review Article

ADVANCED IMAGING

Super-resolution microscopy reveals new insights into organelle interactions

Hongjun Wu,[a,b,c] Yalan Zhao,[a,b,c] Xiao Zhou,[a,b,c] Tianxiao Wu,[a,b,c] Jiaming Qian,[a,b,c] Shijia Wu,[a,b,c] Yongtao Liu,[a,b,c,*] and Chao Zuo[a,b,c,*]

[a]Smart Computational Imaging Laboratory (SCILab), School of Electronic and Optical Engineering, Nanjing University of Science and Technology, Nanjing, China
[b]Smart Computational Imaging Research Institute (SCIRI) of Nanjing University of Science and Technology, Nanjing, China
[c]Jiangsu Key Laboratory of Spectral Imaging & Intelligent Sense, Nanjing, China

Abstract. Fluorescence microscopy technology is a crucial tool in biomedical research, enabling us to visualize the structure and function of tissue cells at the cellular level. Its great potential lies in fluorescence super-resolution fluorescence microscopy, which surpasses the limitations of diffraction and enables high-resolution real-time imaging of nano-subcellular structures, including organelles and cell matrices. It, therefore, contributes significantly to exploring disease mechanisms, ranging from the exchange of protein aggregates at a structural level to the identification of morphological defects in organelles. In this review, we first provide an overview of the principles of various super-resolution microscopy techniques. We then delve into the intricate transmembrane interactions exhibited by membrane organelles, as well as the intricate information communication within membraneless organelles in both physiological and pathological conditions. Finally, we examine the evolution of super-resolution technology and discuss its application in biomedicine. Overall, this review briefly introduces the principles of super-resolution microscopy and highlights its novel results in organelles to guide its application in the biomedical field.

Keywords: organelles; interaction effects; cellular responses; super-resolution microscopy; bioimaging.

Received May 31, 2024; revised manuscript received Aug. 19, 2024; accepted Sep. 18, 2024; published online Nov. 14, 2024.

[DOI: 10.3788/AI.2024.20004]

1. Introduction

The cell is the basic unit of body structure and function composed of different organelles and the cytoplasmic matrix. The biological activities of cellular molecules are illustrated by microscopies[1]. Due to the limitations of traditional bio-techniques, micro-phenomena in cells such as the principle, active expression, and ultrastructure of organelles cannot be directly observed[2–4]. With the development of optical microscopies, it makes it possible for scholars to observe organelles such as mitochondria, lysosomes, and ribosomes to reveal important biomedical problems such as cell division, cell differentiation, cell aging, cell death, and interaction effects. For example, tumor cells are characterized by vigorous growth, high proliferation, and division with malignant cells posing a risk of metastasis[5]. As a result, the antitumor effects often yield unsatisfactory results due to multi-drug resistance and side effects[6]. To improve the antitumor effects, research focusing on targeting organelles like mitochondria, lysosomes, and endoplasmic reticulum has explored the relationship between the cellular responses and interaction effects of organelles[7]. Nano-organelles cannot be imaged by traditional microscopy due to diffraction limitations, resulting in the loss of fine structural and functional information. Fluorescence microscopy, however, could break the limitations of traditional microscopy, which has been used in biochemistry and life sciences widely. However, it also faces daunting challenges in quantitative evaluation for nano-organelles, which will limit function tracing, protein quantification at the unit point, and microstructural changes. Then, super-resolution fluorescence microscopy (FLSR) provides super-resolution and rapid imaging for precision medicine. It realizes the

*Address all correspondence to Yongtao Liu, yongtao.liu@njust.edu.cn; Chao Zuo, zuochao@njust.edu.cn

bidirectional or multi-directional combination of optical technology with fluorescent probes, fluorescent dyes, or fluorescent nanoparticles. The resolution is approximately 5 to 100 nm, which has obvious advantages in organelle interaction and has obtained original and novel results in basic biomedical research such as cell biology, immunology, and pathological pharmacy[8]. Super-resolution methods can also be identified by three well-known methods, including single-molecule localization, stimulated emission depletion (STED), and structured illumination.

Stochastic optical reconstruction microscopy (STORM) is a type of single-molecule localization technology, in which the state of fluorescence is changed by a special dye with a light control switch[9]. The imaging resolution of STORM is about 10 to 30 nm, which is suitable for organelles including structure and function such as the fission and fission of mitochondria[10] and neuronal cytoskeletons[11]. However, continuous flashing is required during the process of this technology, and as a result, the cumulative effect increases its phototoxicity. Therefore, it is not applied in living cells. STED microscopy combines confocal microscopy with the stimulated radiation characteristics of fluorophores to achieve super-resolution imaging[12]. Its imaging resolution has improved to the nanometer level, which can realize structural and functional information for nano-molecules. This technology was applied to assess the changes in lipid bilayer and information communication in living cells[13]. Meanwhile, the changes of different states for photon energy shortly are indispensable. The parameters of the laser such as high power and short pulse width are important. Based on structured light illumination, structured illumination microscopy (SIM) has the advantage of fast and long-term analysis for monolayer living cells especially. The structural information in living cells is acquired by different types of SIM[14,15]. The axial resolution of about 500 nm limits its application in thick samples such as organoids. MINFLUX combined with single-molecule localization microscopy (SMLM) and STED has the advantages of higher lateral and axial resolution with fewer fluorescent molecules[16]. It achieves super-resolution images in three dimensions, but related research, such as cellular tracking, is from two-dimensional space[17,18].

In this review, we first introduce key super-resolution technologies for organelle research, such as STORM, STED, SIM, and MINFLUX. Then, the application and development of organelle interaction effects with FLSR are systematically described. Finally, we briefly summarize the research on the interaction effects between two or more organelles by FLSR, providing scientific proofs for basic research.

2. Fluorescence Super-Resolution Imaging Technologies

2.1. Single-Molecule Localization Microscopy

SMLM regulates the amount of luminescence of fluorescent molecules around the diffraction-restricted region, the result of which is that fluorescent molecules are aligned one by one. The principle of STORM is shown in Fig. 1(a)[9]. The technique takes advantage of the photoconversion properties of fluorescent molecules to obtain fluorescence signals at different points one by one. The optical path and spectral modulation of STORM are shown in Fig. 1(b). The intensity and switch characters are changed by an acousto-optic tunable filter (AOTF) to alternate illumination of the excitation wavelength and emission wavelength. Based on the system of SMLM, total internal reflection fluorescence (TIRF) is used to increase SNR. One of the key elements is the single-molecule localization algorithm. The sample is labeled by a specific fluorescent molecule probe with photon-switching characteristics, which could be exchanged by optical elements. Multimolecular fluorescence images spatially are separated into a series of sub-images so that there is only a small amount of sparsely distributed single-molecule emission fluorescence in each frame. A single molecule effectively avoids the influence of the light diffraction limit, and its center position is determined by the single-molecule localization algorithm. Finally, a super-resolution image is reconstructed by every positioning point. There are some important elements for single-molecule localization imaging. The first one is light-conversion fluorescent probes. Fluorescent molecules are separated from others by photoconversion fluorescent molecules. Common fluorescent probes include organic synthetic anthocyanin dyes and photoactivated fluorescent proteins. The second one is the accurate single-molecule localization and reconstruction algorithm, which directly affects the imaging resolution. It is concluded that the Gaussian function can obtain the best positioning accuracy when fitting the point spread function of the collected single molecule. The third one is high-sensitivity acquisition equipment. Single-molecule signals can be accurately collected by high-sensitivity cameras thanks to the short duration of light-conversion fluorescent probes. SMLM has developed into a variety of technologies with the advancement of technology, such as photoactivated localization microscopy (PALM), STORM, and combined multiple techniques with microscopy. The imaging resolution of SMLM is about 10–30 nm, which is lower than some subcellular structures. The precise localization analysis of nanoscale biomolecules can be performed by the technology. Betzig *et al.*[19] utilized activated light to regulate the activation state of a single fluorescent molecule during the activated period, which was shortened as PALM for the first time. Meanwhile, Zhuang *et al.*[9] designed a novel SMLM technology named STORM. With the discovery of some dyes spontaneously flashing in specific chemical environments, direct stochastic optical reconstruction microscopy (dSTORM) was developed[20],

$$\hat{x}_0 = a^{-1}\left[\left(\sum_{j\in D} s_j\omega_j b_j\right)\left(\sum_{j\in D}\omega_j\right) - \left(\sum_{j\in D}\omega_j b_j\right)\left(\sum_{j\in D} s_j\omega_j\right)\right], \tag{1}$$

$$\hat{y}_0 = a^{-1}\left[\left(\sum_{j\in D} s_j\omega_j b_j\right)\left(\sum_{j\in D}\omega_j\right) - \left(\sum_{j\in D}\omega_j b_j\right)\left(\sum_{j\in D} s_j^2\omega_j\right)\right], \tag{2}$$

$$\langle\langle\Delta x\rangle^2\rangle = \frac{2\sigma^2 + a^2/12}{N} + \frac{8\pi\sigma^4 b^2}{a^2 N^2}. \tag{3}$$

The imaging resolution of STORM is dependent on the accuracy of the single-molecule localization theoretically. The localization accuracy, size, and density of fluorescent probes directly affect the spatial resolution. Resolution can be further increased with a smaller fluorescent probe, which determines the Gaussian width of the point spread function (PSF). One of the

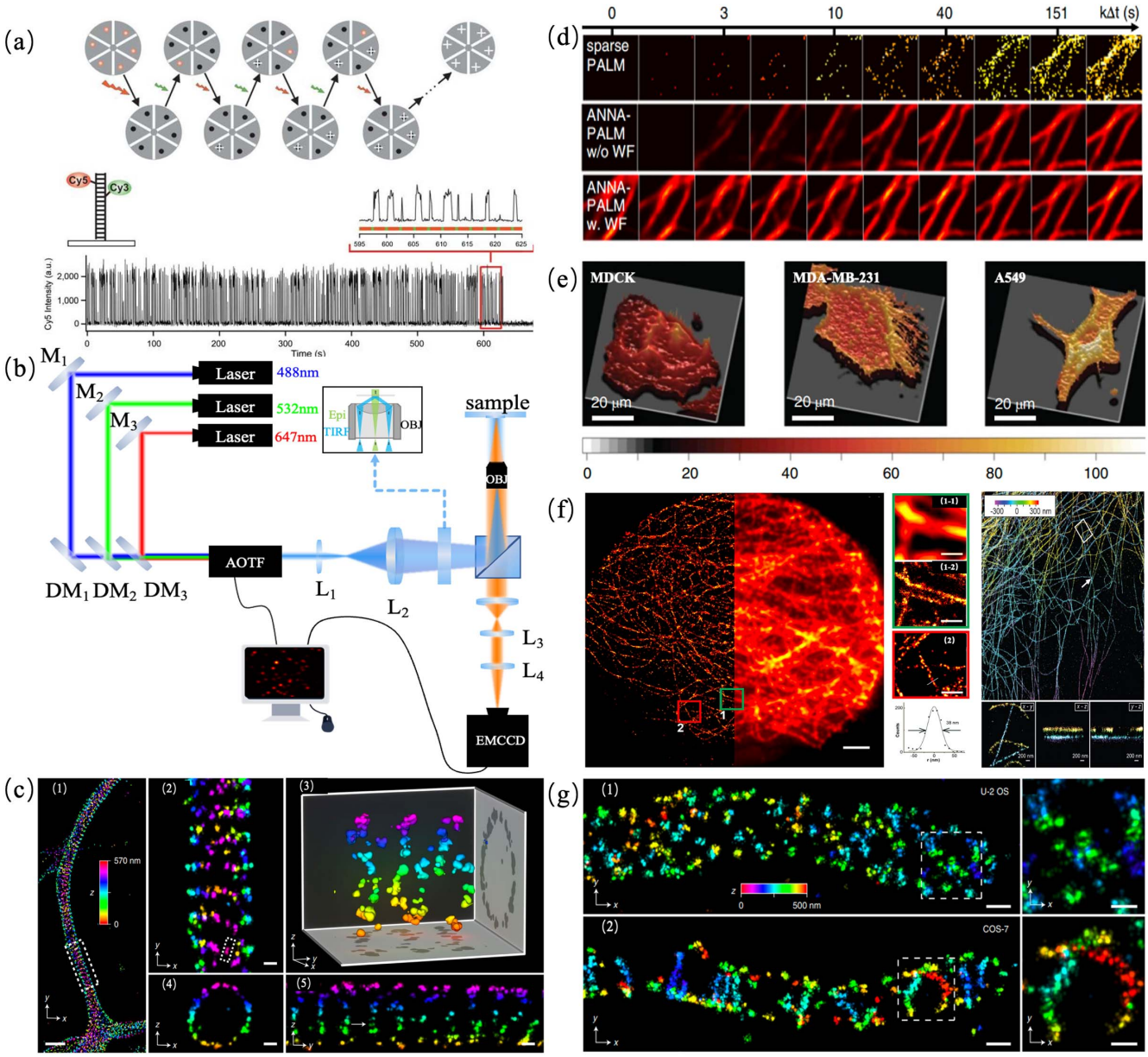

Fig. 1 The basic principle and application of SMLM. (a) The basic principle of STORM[9]. (b) Optical path and spectral modulation process of traditional STORM. (c) 4Pi-STORM imaging of the neuronal cytoskeleton[11]. (d) The process of image reconstruction based on a deep learning network. (e) Comparison of basal membrane profiles of three different cell types[25]. (f) STORM (left) and wide-field (right) images of microtubules in HepG2 cells labeled with 565 quantum dots (QDs)[10]. (g) 4Pi-STORM imaging of mitochondrial crista in the U-2 OS cell and COS-7 cell, respectively[11].

traditional locations is the least squares method, and the center of localization is explained as Eqs. (1)–(3). The image is rebuilt by numerous frames of a single fluorescent molecule, and the density of the fluorescent probe has an important influence on image resolution. Huang *et al.*[21] added a column lens to the imaging optical system that changed the received shape of the PSF to restore the axial localization information, and its axial resolution and imaging depth finally reached 50–60 and 600 nm, respectively. Meanwhile, bio information could be thoroughly collected by two opposing objectives of 4Pi microscopy to get the localization accuracy. In 2022, STORM combined with 4Pi microscopy improved the axial resolution and imaging depth to 5 and 600 nm, respectively[11]. The results of 4Pi-STORM imaging not only showed the neuronal cytoskeleton but also distinguished the mitochondrial crista in the U-2 OS cell and COS-7 cell, respectively, as shown in Figs. 1(c) and 1(g). When the excitation density of each frame was increased to reduce the total time, the temporal resolution was improved. Zhu *et al.*[22] applied a compressed sensing algorithm that effectively increased the excitation density of each frame, the temporal resolution of which improved to 3 s in imaging microtubule dynamics in living cells. In addition, materials scientists

have found that the distance of ionic coupling between fluorescent molecules and materials could achieve the axial localization and imaging speed of fluorescence. Jones *et al.*[23] monitored clathrin-coated pits (CCPs) labeled with various probes to explore the endocytosis of transferrin for living cells, and the temporal resolution and lateral resolution were improved to 0.5 s and 20 nm, respectively. QDs, a type of photoluminescent material with the advantages of strong photostability, high quantum yield, strong quenching resistance, and good biocompatibility, are regarded as ideal fluorescent probes for STORM. The images of microtubules in HepG2 cells labeled with 565 QDs were imaged by STORM[10], and the lateral resolution was increased to 24 nm, as depicted in Fig. 1(f). Ouyang *et al.*[24] used the deep learning method to reduce the total number of imaging frames from 30,000 to 300 frames, and the imaging speed of STORM was significantly improved. The imaging depth was around 100 and 25 nm for metallic gold and graphene, respectively[25], which could achieve discrimination basal membrane profiles for different cells, as illustrated in Fig. 1(e). In conclusion, the improved STORM opens up new avenues for characterizing cellular ultrastructures in living cells.

2.2. Stimulated Emission Depletion

In 1994, STED was first designed by Hell and Wichmann. The basic principle of STED is shown in Fig. 2(a)[12]. The image is based on the pixel-by-pixel, which is similar to CLSM. Another light could quench excited fluorophores and keep the intensity at the center, which is named the donut-shaped spot. However, there is a pinhole in front of the detector, and the peripheral fluorescence of the first light is depleted by the second spot. As a result, the imaging resolution is increased rapidly. Photons from the laser are absorbed by fluorophores, and the status of fluorescence is brought from the ground singlet (S0) to its first excited singlet electronic state (S1). The fluorophores of samples are switched multiple times during the whole process. The traditional method is

$$d \approx \lambda / \left(2\mathrm{NA}\sqrt{1 + I/I_{\mathrm{s}}}\right). \tag{4}$$

Here, NA, I, and I_{s} denote the numerical aperture of the lens, the focal peak intensity at the donut crest, and the intensity that reduces the fluorescence ability by half, respectively[26]. FLSR provided more structural and functional unseen details for the subcellular level. Importantly, STED makes up for the margin between EM and confocal laser scanning microscopy (CLSM), the optical path of which was more complex than that of others, as shown in Fig. 2(b)[27]. For example, Liu *et al.*[28] improved STED resolution to 30 nm based on super-linearity of upconversion nanoparticles at low power. At present, the technology of STED has been used to explore the finest details in numerous directions of biomedicine as shown in Fig. 2(e)[29]. As we all know, STED has been successfully imaged in thin samples, such as single cells, and tissue sections. But the advantage of the super-resolution was limited in the *Z*-axis. STED combined with other technologies was designed to increase its sensitivity, specificity, and so on. Gould *et al.*[30] first implemented adaptive optics (AO) in STED to acquire the three-dimensional (3D) super-resolution information of zebrafish retina sections with a thickness of more than 14 m. A low signal-to-noise ratio is the major element for STED because of high-power depletion. Zdańkowski *et al.*[31] demonstrated STED with automated aberration correction to improve the image resolution, and its depth was verified in the field of axons in differentiated induced pluripotent stem cells growing with a thick layer of 80 m. To decrease the photodamage, Wang *et al.*[32] modulated information from the temporal and spatial domains, and imaging resolution improved by 100 nm for fixed and living cells. Patton *et al.*[33] proposed an AO scheme with two correction elements and included DM and SLM to correct aberrations in all beam paths, which could realize the complex structures in the Drosophila brain with a depth of 15 m. Gao *et al.*[34] compensated for the phase aberration of the system based on an aperture segmentation-based method and achieved imaging for fluorescent polystyrene beads with a diameter of 40 nm. Kuang *et al.*[35] approached fluorescence emission difference microscopy (FED) on the autophagy-associated proteins (LC3) labeled by green fluorescent protein (GFP) in HEK293 cells, in which the spatial resolution was reduced to less than λ/4 in the far field, and the dwell time was shortened to 0.3 s at every pixel. This method did not require the precise alignment of two laser beams, where I_c, I_n, and I_{FED} are the normalized intensity distributions of the confocal, negative confocal, and FED images, respectively, and r is the subtractive factor,

$$I_{\mathrm{FED}} = I_c - r \cdot I_n. \tag{5}$$

In addition, the differential resolution of FED combining the nonlinear effects of the upconversion nanoparticles was improved observably[36–38].

The exchange of the substance and interaction effect in live cells needs to have high performance, such as real-time, fast, and super-resolution characteristics. Hedde *et al.*[13] combined raster image correlation spectroscopy (RICS) with STED to monitor the status of the lipid bilayer labeled with Atto647N-DPPE, which significantly improved the spatial resolution and sensitivity at low fluorophore concentration, as demonstrated in Fig. 2(c). In 2021, Wang *et al.*[39] proposed FM-STED based on frequency spectrum modulation, avoiding severe photo-damage or photobleaching, which had been confirmed in fluorescent beads and microtubules, as depicted in Fig. 2(f). Therefore, researchers have tried to develop it in modern life science. Zhang *et al.*[40] incorporated fluorescence *in situ* hybridization (FISH) into STED to improve its sensitivity, the result of which clarified the distribution and kinetic mechanisms of intracellular mRNA molecules by labeling the mRNA of presynaptic proteins in primary hippocampal neurons. Plasmodium is an important factor for malaria, but its small size and high sensitivity to light make it impossible to study *in vitro*. Schloetel *et al.*[41] designed guided STED based on AO, which could avoid the damage of the high power of plasmodium, effectively monitoring the whole plasmodium life cycle with a resolution of 35 nm. In 2020, Wang *et al.*[42] put forward digitally enhanced STED (DE-STED) to decrease the influence of depletion power based on the donut image, achieving a spatial resolution of λ/8 at a depletion power of 1.4 mW. It limits optical techniques in achieving deeper imaging depth because of light scattering. Presynaptic long-term potentiation (LTP) plays an important role in learning and memory. However, it is difficult for traditional imaging recording methods to study its mechanism. In 2023, Fukaya *et al.*[43] used STED to analyze the Munc13-1 and RIM1 molecules in the active region of hippocampal mossy fiber synapses, and the super-resolution imaging showed that

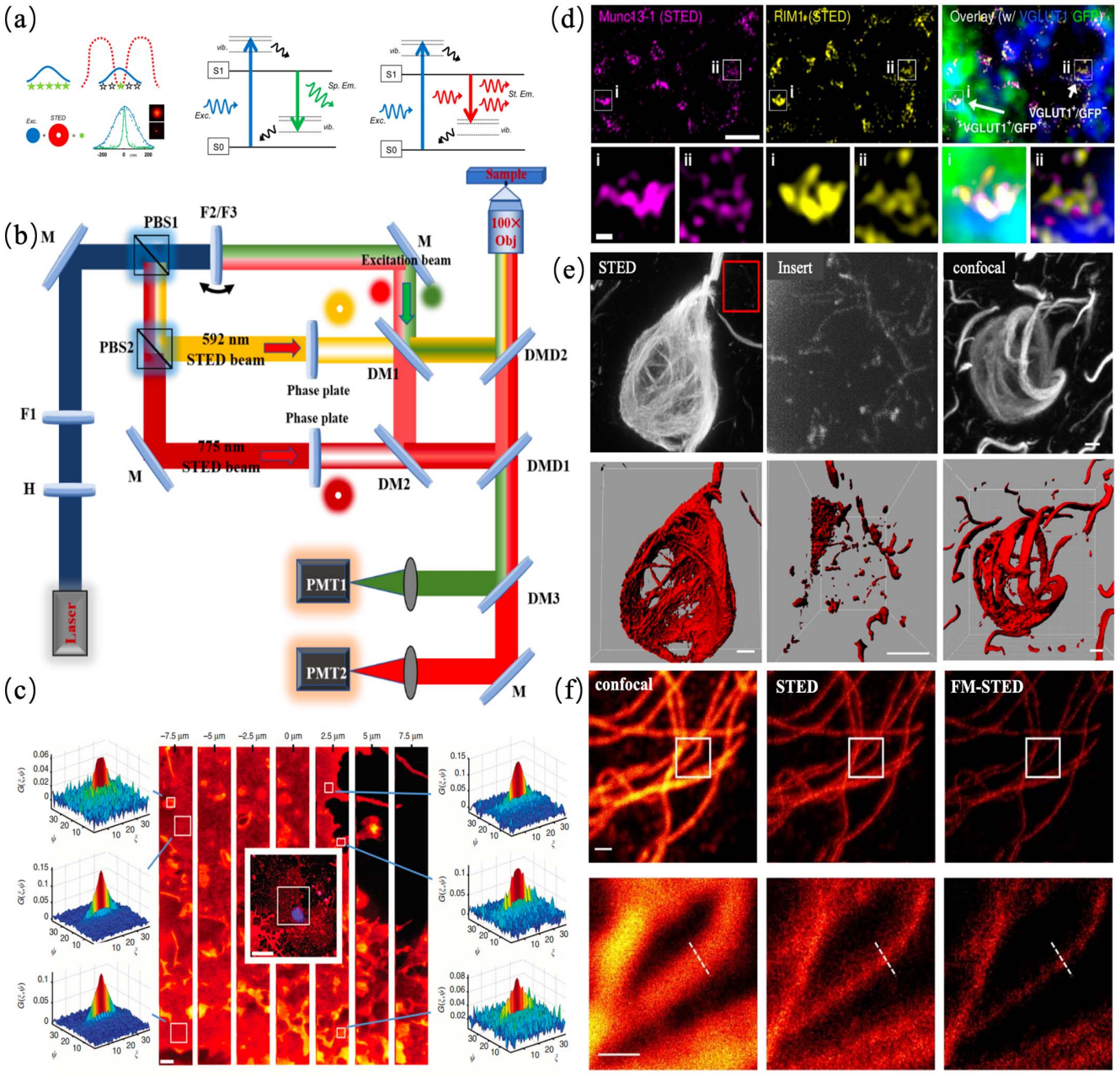

Fig. 2 The basic principle and application of STED. (a) The basic principle of STED[12]. (b) Optical path and spectral modulation process of two-color STED[27]. (c) Diffusion of Atto647N-DPPE in the membrane of an XTC cell in STED[13]. (d) Immunolabeled Munc13-1 and RIM1 molecules were visualized by STED microscopy at the hMFBs[43]. (e) Diagnostics and understanding disease mechanisms in STED and confocal microscopy[29]. (f) The imaging of microtubules in fixed BSC-1 cells in confocal microscopy, STED, and FM-STED[39].

the number of molecules increased after tetanic stimulation, as shown in Fig. 2(d). It indicated that components in the active zone were related to fusion ability and synaptic vesicles during LTP. More importantly, STED provided a novel imaging method for the dynamic processes of live cells with nanometer scales. Velasco *et al.*[44] combined two-photon excitation, AO, red-emitting organic dyes, and a long-working-distance water-immersion objective lens to achieve the imaging of brain tissue up to 164 μm in fixed mice and 76 μm in living mice. As we all know, STED acquired super-resolution based on high depletion power. As a result, severe phototoxicity or photobleaching made it difficult to apply for live cells. Zhang *et al.*[27] designed a low-power two-color STED super-resolution microscope based on digital enhancement technology, which achieved high-quality imaging for mitochondria and microtubules in live cells. Fluorescent dyes are indistinguishable at multiple channels by conventional methods. Abberior proposed the TIMEBOW method that separated the lifetime of the excited

state, improving the accuracy of four channels excited by one wavelength laser[45]. In 2023, Bucevičius *et al.*[46] exploited the dyes' structural diversity for the selection of highly biocompatible probes, and successfully applied them in STED in live cells and tissues.

2.3. Structured Illumination Microscopy

SIM is a super-resolution microscopy imaging technique based on frequency domain regulation, which was first proposed by Gustafsson[47]. The basic principle is the stacking gate effect excited from fluorescent samples by intensity sinusoidal modulated structured light. The high-frequency information away from far-field space is encoded to the low-frequency microscopy image, which achieves super-resolution optical microscopy imaging that breaks through the Abbe diffraction limit. The multilevel spectrum carrying sample information is generated because of the convolution of the illumination pattern spectrum when the sample is excited by sinusoidal structured light. The high-frequency portion is detected within the cutoff frequency range of the system when the spectrum level is ± 1, as shown in Fig. 3(a). Since this high-frequency information is added to the low-frequency information, the reconstruction of the high-frequency components is decoded through a series of post-processing algorithms[48]. Multiple fluorescence images with different phase shifts are collected at the same direction angle, and those equations are solved to separate and reorganize the multiple harmonic terms in the spectral space. Finally, super-resolution images are reconstructed with multiple raw images at different directions or different phases.

Since the sample of SIM was limited by the diffraction limitation before laser irradiation, its maximal grating frequency increased to double the width of the cutoff frequency. At present, this imaging resolution of SIM improved to 100 nm[50]. Although the lateral resolution of SIM is not as good as PALM, STORM, STED, and other technologies, it is very suitable for super-resolution imaging of live cells because of its advantages such as high photon efficiency, fast imaging speed, and

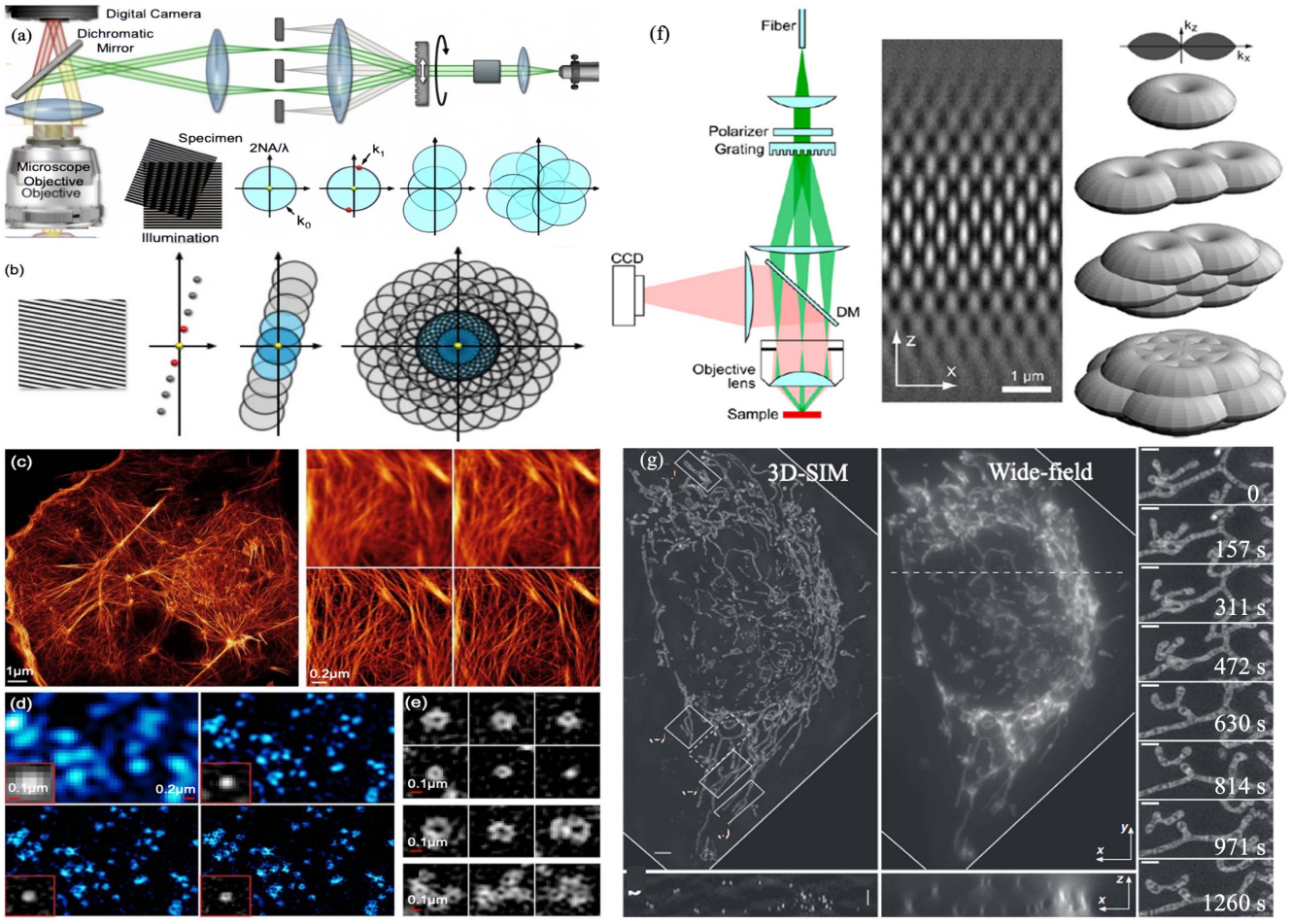

Fig. 3 The basic principle and application of SIM. (a) Optical path and spectral modulation process of traditional SIM (linear). (b) Spectral modulation process of SSIM. (c) F-actin protein of COS-7 cells imaged by SSIM and other methods (top left: wide field, top right: deconvolution, bottom left: SIM, bottom right: SSIM)[14]. (d) The structure of mesoplasmic membrane microcapsules in COS-7 cells from different methods (top left: wide field, top right: deconvolution, bottom left: SIM, bottom right: SSIM)[14]. (e) The SSIM image of mesoplasmic membrane microcapsules in live COS-7 cells[14]. (f) The basic principle of 3D-SIM[21]. (g) Imaging results of traditional widefield and 3D-SIM in live HeLa cells[49].

full-field imaging mode. Huang *et al.*[51] proposed the Hessian constraint based on the spatiotemporal continuity of biological samples, which effectively reduced the reconstruction artifacts generated during SIM post-processing. The dosage of photons was reduced to 90%, which promoted long-term super-resolution imaging of moving vesicles in the endoplasmic reticulum with a spatiotemporal resolution of 88 nm and 188 Hz. Gustafsson[52] further proposed the saturated structure illumination apparent microtechnology (SSIM) based on fluorescence saturation, which achieved higher lateral resolution (50 nm). The surface of samples was excited by local fluorescence at high-power sinusoidal light of SSIM, emitting a non-sinusoidal rectangular grating pattern, and the principle was presented in Fig. 3(b). Hesper Rego *et al.*[53] achieved its lateral resolution of 50 nm with reversible optical switching fluorescent proteins. However, the photobleaching was increased under the high-intensity light of SSIM, which made it difficult to apply to live cell imaging. Li *et al.*[14] combined photo-sheet microscopy with a light-activated fluorescent protein to decrease the phototoxicity, which performed long-term dynamic observations of living cells, such as in Figs. 3(b)–3(e). Huang *et al.*[21] designed three-dimensional structure illumination microimaging technology (3D-SIM) to obtain the 3D structure of cells. A beam of interference light was added to the SIM system to generate a 3D illumination light field. The optical transfer function was transported to achieve twice the axial super-resolution in the axial direction. The spectrum of the sample was moved in the lateral direction, the result of which was that lateral resolution and axial resolution were 100 nm and 280 nm, respectively, as shown in Fig. 3(f). 3D-SIM still cannot achieve isotropic super-resolution because the axial resolution of wide-field fluorescence microscopy is only one-third of the lateral resolution. Shao *et al.*[54] combined SIM with 4Pi technology named I5S, realizing 100 nm in both lateral and axial directions. Then, Shao *et al.*[49] achieved 3D imaging of live cells at a rate of 5 s/frame with the spatial light modulator, as illustrated in Fig. 3(g).

2.4. MINFLUX

MINFLUX is a super-resolution technology that combines the advantages of STED and SMLM, which was first proposed by Stefan Hell in 2014. MINFLUX separates fluorophores based on SMLM, but the light field with minimal central intensity was applied such as the donut of STED[16]. Compared with other super-resolution technology, it could locate the fluorophore with faster and higher precision. It enables the highest possible resolution in fluorescence microscopy with a minimum molecule of 1–3 nm. More importantly, the number of fluorescent photons is less than 100–300 times with an accuracy of 1 nm. The role of the donut in MINFLUX is used to excite the fluorescence that is completely different from STED. If the center of the donut coincides perfectly with the fluorophore, fluorescence could not be monitored. On the contrary, fluorescence intensity is detected by the monitor. As a result, this special positioning method reduces the number of photons required for localization and improves positioning accuracy. The actual donut laser only needs to be irradiated twice to precisely locate the precise light-emitting position of the fluorescent molecule in one dimension. The smaller the moving distance is, the higher the final positioning accuracy will be. MINFLUX can accurately locate single-molecule fluorescence through the fluorescence intensity obtained after moving 3 positions at two dimensions, as shown in Fig. 4(a). To avoid the background noise, it needs to add a center position in practice. Meanwhile, there are slight differences between MINFLUX and SMLM, as shown in Fig. 4(c).

It has been applied in the fields of biomolecules and neuroscience, bringing technological innovation to mankind. The feature of MINFLUX is high spatial and temporal resolution, which promotes the efficiency of the location of single fluorescent molecules. MINFLUX, a technological innovation, has become more prominent in molecular imaging at the nanoscale. To simplify systemic setup and amplify the lifetime of fluorescence, Masullo *et al.*[55] designed pulsed-MINFLUX (p-MINFLUX) based on the highly photon-efficient single-molecule localization method with a resolution of 2 nm. DNA point accumulation for imaging in nanoscale topography (DNA-PAINT) is a type of super-resolution technique, the principle of which is complementary pairing between DNA molecules. The DNA molecule was labeled by a special target and combined with a complementary DNA molecule. These probes were added and removed orderly to achieve high-resolution imaging. Compared with other SMLMs, DNA-PAINT achieved high specificity and dynamic imaging for target proteins such as intracellular and extracellular protein interaction[56], cell signaling pathway communication[57], and cell molecular dynamics[58]. However, this technique was challenged in multicolor imaging due to the instability of the probes and the crossing of multichannels. To get super-resolution in all three dimensions, Zähringer *et al.*[59] combined p-MINFLUX with DNA-PAINT and provided the switching mechanism of precise localization and high-resolution imaging for DNA origami. The advantage of MINFLUX could achieve high resolution in three dimensions to achieve molecular imaging. Schmidt *et al.*[17] applied MINFLUX to analyze subcells and different nerve cells, finding that the resolution could attain less than 1 nm after 2500-photon yield, as shown in Figs. 4(b) and 4(e). More importantly, it is possible for a plasma membrane system to monitor the communication between organelles, as depicted in Figs. 4(f) and 4(g)[18]. Masullo *et al.*[60] presented RASTMIN, which was an alternative to MINFLUX in single-molecule tracking and high resolution for DNA origami structures. MINFLUX has limitations in multichannel imaging. Ostersehlt *et al.*[61] applied DNA-PAINT with MINFLUX to exemplify the multiple molecular targets of mitochondria in human cells. Zhao *et al.*[62] simulated the two-photon MINFLUX and improved the width of the confidence interval to half of the original thanks to the nonlinear effect of two-photon excitation. Balzarotti *et al.*[16] put forward the basic concept of MINFLUX and detected the precise curves of a single ribosomal subunit in 77 independent tracks in live E. coli bacteria imaged by MINFLUX with a spatial resolution of 20 nm, as shown in Fig. 4(d). Meanwhile, the lateral resolution of MINFLUX achieved 1 to 20 nm, but its axial resolution was greatly reduced to 50 nm. As a result, it is not suitable for 3D imaging. Different from the traditional illumination method, rapid on-site evaluation (ROSE) has a better optical sectioning mode that could obtain the 3D structure information and spatial distribution. Especially, ROSE achieved accurate and rapid diagnosis of pathological sections[63]. Based on this principle, the researchers developed ROSE-Z, which successfully analyzed the hollow structure of the intracellular microtubule diameter from three dimensions. In addition, ROSE could provide powerful techniques for 3D nanostructures, which was successfully applied in multicolor imaging and thick samples. Notably,

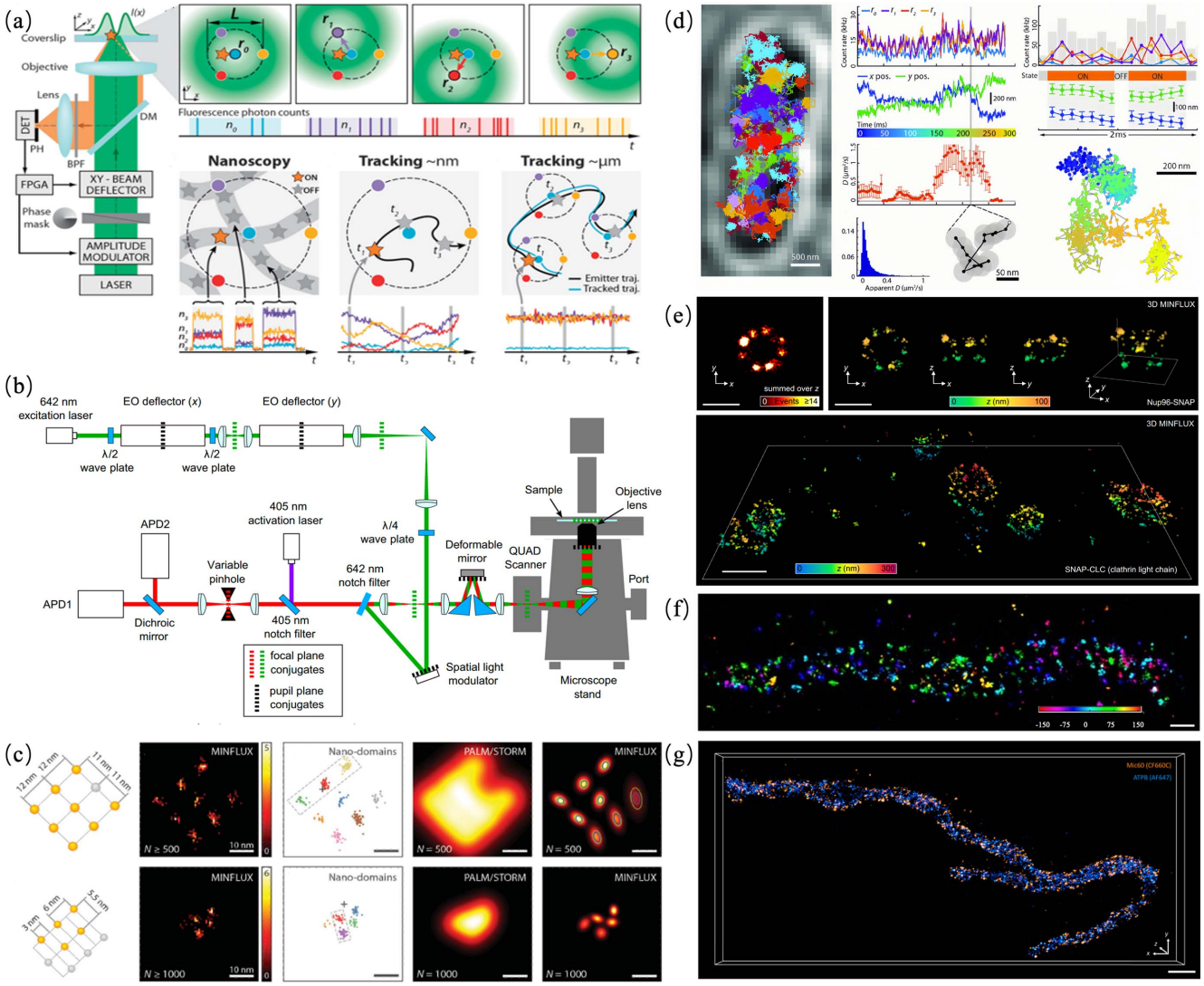

Fig. 4 The basic principle and application of MINFLUX. (a) The basic principle of MINFLUX[16]. (b) Optical path and spectral modulation process of 3D MINFLUX[17]. (c) Arrangement of up to nine on-off switchable fluorophores on the origami (top) and the smaller DNA origami structure (bottom)[16]. (d) Single-molecule MINFLUX imaging and precise tracking in live E. coli bacteria[16]. (e) 3D MINFLUX raw data and corresponding information at different dimensions (top) and clathrin visualized by SNAP labeling in HeLa cells (bottom)[17]. (f) Distribution of Mic60 in mitochondria of human U-2OS cells[18]. (g) Two-color 3D MINFLUX acquisition of a mitochondrion in human dermal fibroblasts[18].

ROSE needed large amounts of data during the acquisition and reconstruction process. It tends to static biological samples. The low optical power of MINFLUX enables real-time imaging at low power, which is suitable for dynamic biological activities. Super-resolution microscopy has the advantages of high resolution, rapid speed, and visualized zoom of structural and functional imaging for biological samples, which promotes the development of modern precision medicine. For example, the morphology and interaction effects of organelles such as mitochondria, lysosomes, and endoplasmic reticulum could be easily imaged by super-resolution microscopy. It is convenient for basic biomedicine to research more biological information, which has a broader prospect and far-reaching significance in organelle research and physiological pathological phenomena.

MINFLUX, a super-resolution microscopy technique, has significant advantages in biomedical research such as the structure and function of neurons, the mechanism of antitumor drugs, and the localization of signal proteins during the exchange of cellular substances. The system itself is more complex due to the combination of the advantages of STED and SMLM. Meanwhile, the high cost of MINFLUX cannot be ignored. It has high requirements for sample preparation including labeled substances and experimental protocols, which greatly increases the complexity and time for researchers. There is still a lot of potential for MINFLUX to promote the research of life sciences and medical diagnosis.

In conclusion, we compared the parameters of each super-resolution technique, and each one has advantages and

Table 1 System Parameters of Different Techniques.

FLSR	PALM/STORM	STED	SIM	MINFLUX
Speed	Thousands of exposures	Point scanning	Full-field imaging	10 kHz
Energy (W/cm^2)	~10^3	~10^7	~10^2	~1
Temporal resolution (ms)	1.2×10^6–1.8×10^6	50	1–100	0.1
XY resolution (nm)	20	30–50	65–100	2–5
Z resolution (nm)	50	70	250	2–3
Fluorescent molecules	Photoswitchable	Free	Free	Photoswitchable
Live cell imaging	Yes	Yes	Yes	Yes
Depth (μm)	0.2	120	20	1
Image reconstruction	Required	Not required	Required	Required

disadvantages, as shown in Table 1. It is very important for image acquisition and reconstruction to maintain a high signal-to-noise ratio (SNR), which could improve the image quality, accuracy, and efficiency of information transmission and optimize the effect of data processing algorithms. STORM achieves super-resolution imaging based on the stochastic activation of single-molecule fluorophores and precise localization by Gaussian fitting. However, localization errors were increased by insufficient photons, which directly affected image reconstruction quality and resolution. Meanwhile, the mislocalization of molecules and image artifacts may occur because of the low SNR. STED enhanced optical resolution by suppressing the expansion of the fluorescence emission area, but the depletion region's boundaries relied on a high SNR. High SNR is not essential for SIM, but artifacts and distortion are not obviously neglectable problems during image reconstruction especially for live samples. Compared with others, MINFLUX determines the position of the molecule by the relative intensity and has advantages in localization accuracy under low SNR. Biological tissues are inherently heterogeneous and complex, and each technique may have differences in imaging speed, depth, resolution, and photodamage. So it is urgent to optimize super-resolution imaging techniques and obtain higher-quality molecular localization and spatial distribution by artificial intelligence. In recent years, with the development of artificial intelligence technology, algorithms based on deep learning have significantly improved parameters and found more details of biological samples. For example, phototoxicity is the key problem of STED techniques. Ebrahimi *et al.*[64] decreased its dwell time to 3.125% by multi-stage progressive image restoration (MPRNet) which effectively reduced photodamage and improved the imaging speed. Chen *et al.*[65] improved resolution and robustness with fewer photons based on the GAN network. The axial resolution of high-density fluorescent samples was limited by the traditional method. Wu *et al.*[66] inputted single-helix point images into a decoder–encoder network based on CNN, and its axial resolution was improved to 50 nm. Meanwhile, SMLM has low temporal resolution because of plentiful images during reconstruction. It was difficult for STED to monitor the dynamic behaviors of live cells. Nehme *et al.*[67] reduced the number of images by the decoder–encoder network. Li *et al.*[68] applied recurrent neural networks (RNNs) to extract features, and the reconstruction time was reduced by 40%. Speiser *et al.*[69] optimized maximum likelihood estimation (MLE) based on the U-Net network to decrease the reconstruction time. Compared with other super-resolution techniques, SIM could achieve real-time tracking of live cells, but its resolution is difficult for small molecules such as localization and spatial tracking. Shah *et al.*[70] employed a residual encoder–decoder network (RED-Net) to improve lateral resolution and remove artifacts. Chen *et al.*[71] proposed a CR-SIM based on the residual neural network to improve the contrast of images. In order to improve axial resolution, Boland *et al.*[72] used the RCAN network to realize two dimensions to three dimensions.

3. Multiple Organelle Interaction of a Tumor

Super-resolution microscopies have the advantages of real-time visualization, ultra-high temporal resolution, and spatial resolution for biological science, which provide novel methods for basic biomedicine such as organelle membrane junctions, interaction effects, cell response mechanisms, and so on. Organelles with unique local environments and molecules play specific roles in interacting with others, which maintains stable conditions of cells and tissues. Lysosome, a monolamellar membrane organelle, meets the metabolic energy and renews organelle structure by decomposing macromolecular substances[73]. The regulation mechanism of lysosomes combined with intracellular autophagy forms autophagy lysosomes, which regulate the number, morphology, and microenvironment of molecular substances[74,75]. Those play vital roles in biological behavior such as cellular metabolism, phagocytosis, and autolysis. The endoplasmic reticulum (ER) connected with the plasma membrane and the nuclear membrane is involved in the synthesis, processing, packaging, and transportation of proteins and lipids[76]. It plays an important role in various inhibition metastasis pathways such as tumor cell ablation, apoptosis, autophagy, and necrosis. On the one hand, abnormal conditions such as tumor hypoxia, oxidative stress, and low pH conditions enhance the survival and metastasis of tumor cells. On the other hand, folded protein is disordered in the ER, the result of which was that the growth of the tumor was inhibited by endoplasmic reticulum stress (ERS)[77]. It has been confirmed that tumor growth was markedly retained by improving its fluidity[78], fusion[79], and permeability[80]. The Golgi apparatus, an intracellular protein-centric

delivery system, consists of saccules and different vesicles[81]. That facilitates tumor migration, invasion, and angiogenesis. The expanded Golgi apparatus provides convenient conditions for tumor cell metabolism and protein secretion[82]. The activities of organelles and their components directly influence cells' growth, repair, and proliferation abilities. Each organelle not only performs its own function, but also cooperates with others to achieve complex physiological functions regulating the cell status under physiological or pathological conditions such as oxidative stress, metabolism, autophagy, uptake, and escape[83,84]. The cell activity and homeostasis are observably regulated by nano-scale organelles such as mitochondria, ER, microtubules, and lysosomes. Modern biomedicine obtained quick and comprehensive development from the perspective of super-resolution imaging.

Different techniques enable super-resolution imaging of live or fixed cells. For example, it is critical for live cells to choose reactive dyes. In the early phase of staining, cells in the best condition were selected for plating. The density of cells is maintained at 50% to 70% because of interaction effects. The fluorescent probes were diluted by a serum-free medium, the working concentration of which was 100 nmol to 1 mol. The optimal staining time is tested by pre-experiment because of different sensitivities of cells. It is necessary to turn on the live cell culture device in advance to maintain the working temperature. For fixed cells, the immunohistochemical staining process is complex, and the quality of samples is greatly deteriorated. Pre-fixation is required for some special cell structures such as nuclear pores. Conventional fixative solutions damage the cellular structure such as paraformaldehyde or methanol, causing cell water absorption failure and deterioration. Physical fixation such as the frozen method gradually replaces chemical fixation. In addition, it is necessary to eliminate fluorescence artifacts caused by chemical reagents and glass slides. At present, the common methods are sodium borohydride or acid-base treatment. It is noted that a short cleaning with pure water is required before mounting. It availably removes residual reagents to avoid salt precipitation on the surface of the samples. Therefore, a variety of factors should be considered to improve the accuracy and reliability of the super-resolution images in the immunohistochemical staining process.

Here, we review the interaction effects between tumor organelles from the perspective of super-resolution microscopy, including mitochondria, lysosomes, nuclei, endoplasmic reticulum, and Golgi apparatus. This section aims to elaborate on the physiological and pathological phenomena and guide treatment from the subcellular level. Meanwhile, this part systematically analyzes the structural and functional information of organelles by different super-resolution techniques, which promotes the application and development of super-resolution microscopy imaging in oncology.

3.1. The Interaction Effect between Mitochondria and Lysosomes

Lysosomes and mitochondria are important dynamic organelles that are widely involved in many important cellular processes, whose dysfunction is associated with various diseases, such as neurodegenerative diseases, diabetes, cancer, and cardiovascular diseases[85]. Mitochondria with a diameter of 0.5–1.0 μm, a double-membrane organelle, provide the necessary energy for cellular activity through electron transport chains and oxidative phosphorylation reactions[86]. The inner membrane is folded and highly coiled to form the inner cristae, which is in contrast with the outer membrane. Super-resolution microscopy made up for the deficiencies of electron microscopy and traditional fluorescence imaging[86]. Betzig *et al.*[87] first localized mitochondria based on mitochondrial respiratory chain protein cytochrome C oxidase by PALM. The mitochondrial dynamic tube is the basic mechanism for the mitochondrial network, which was driven by the motor protein KIF5B, such as in Fig. 5(a). Consequently, it continuously elongated and combined with others to form the mitochondrial network, while the integrity and function of DNA were damaged[88]. Qin *et al.*[89] used double fluorescent-labeled grazing-incidence SIM (GI-SIM) to perform continuous multi-frame fast super-resolution imaging of mitochondrial tubules. Chen *et al.*[90] realized wide-field imaging during the process of mitochondrial tube fission and fusion labeled by the dithiol chemical bond, and the processing algorithm of the image significantly increased time resolution to 0.8 s, as shown in Fig. 5(c). Morphological changes of mitochondria have also been confirmed by SIM such as in Fig. 5(d)[51]. The TOM complex, the nanometer mitochondrial outer membrane protein, is the main transmission pore of encoded proteins in mitochondria, the spatial distribution of which cannot be located precisely. Wurm *et al.*[91] used STED technology to locate the spatial distribution of Tom 20 in real-time, the result of which was that its distribution followed a gradient from the perinuclear to the peripheral mitochondria. Donnert *et al.*[92] achieved co-localization of TOM 20 and ATP synthase by two-color STED microscopy with a resolution of 5 nm. The structure of the mitochondrial inner cristae, about 100 nm, was imaged by isoSTED with a spatial resolution of 30–40 nm[93]. Huang *et al.*[51] realized the real-time imaging of the mitochondrial structure transfected with GFP by SIM, which realized the visualization during the dynamic process of mitochondrial fission and fusion. Lysosome is a single-layered vesicle organelle with various shapes, the diameters of which are from 0.025 to 0.8 μm. It removes damaged organelles and cellular metabolites through the endocytosis effect, which maintains normal metabolism[73]. Fang *et al.*[94] designed a fluorescent nanoprobe with high selectivity, photostability, and low cytotoxicity, which realized real-time tracking imaging of lysosome dynamics and its uptake ability by SIM, such as in Fig. 5(b).

As membrane-structured organelles, morphological regulation and bioinformation usually communicate by the membrane–membrane contact site (MCS). Deficiency of the MCS reduces mitochondrial tethering, which defects its functional characteristics. Calcium ion is an important biological molecule in cell activity, the concentration of which has a direct effect on cell apoptosis, mitochondrial metabolism, and ATP synthesis. Mitochondria are important regulators of calcium ions, and their homeostasis is closely related to the uptake of internal calcium ion pairs. Transient receptor potential mucin channel 1 (TRPML1) was regarded as an important point for the interaction between lysosomes and mitochondria to regulate ion transfer, as shown in Fig. 5(f)[83]. The average distance between mitochondria and lysosomes is about 10 nm in normal conditions; therefore, the light diffraction limit of traditional fluorescence microscopy makes structural imaging impossible. Wong *et al.*[95] demonstrated that the formation and unbinding of the MCS between mitochondria and lysosomes occurred simultaneously, and the dynamic homeostasis of fission and fusion was regulated by their MCS. Studies have found that Rab7 also

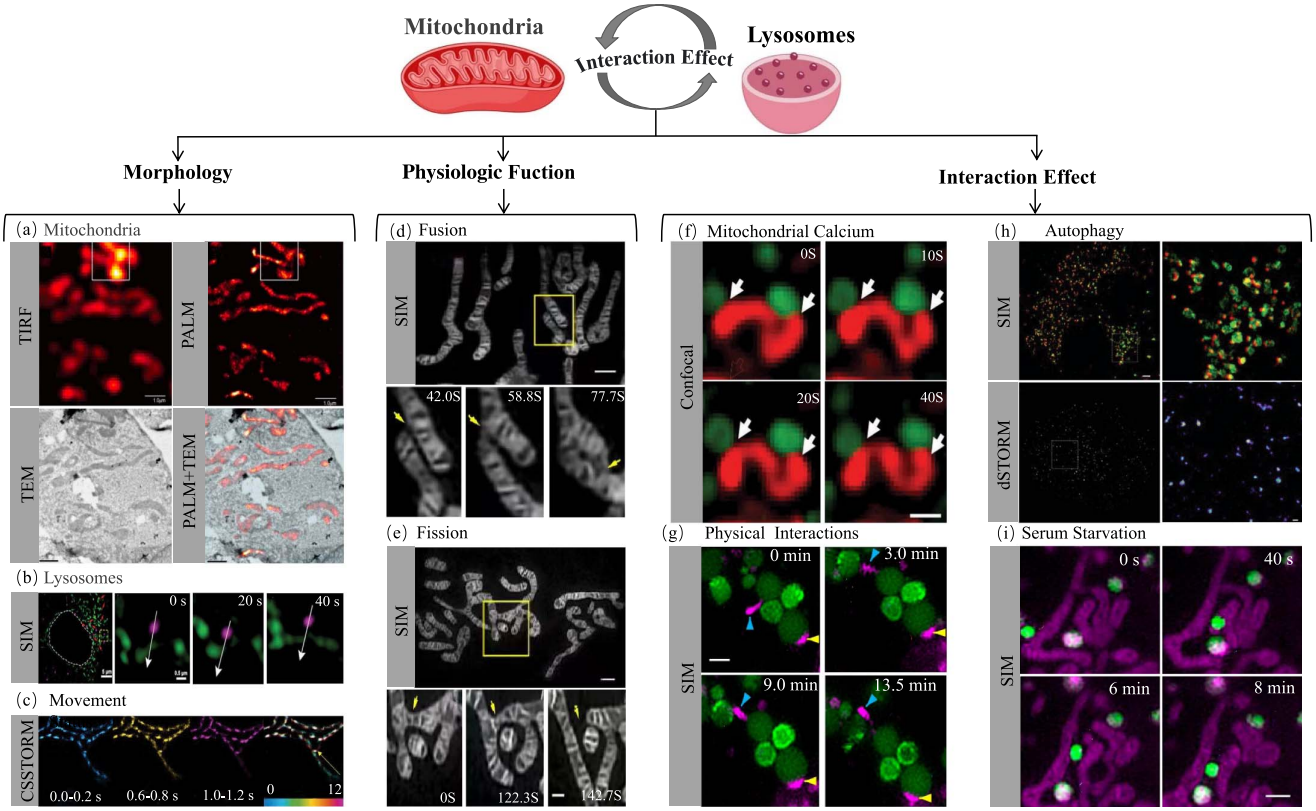

Fig. 5 The properties and interaction of mitochondria and lysosomes. (a) Comparative summed-molecule TIRF, PALM, TEM, and PALM+TEM overlay images of mitochondria in a cryo-prepared thin section from a COS-7 cell expressing dEosFP-tagged cytochrome-C oxidase import sequence[87]. (b) SIM image of lysosome in HeLa cell magnified images from the dashed box at different time points[94]. (c) The movement status of mitochondria at different time points (left) and the whole tubulation retraction process (right) were imaged by STORM[90]. (d) The fusion of two mitochondria[51]. (e) The fission of one mitochondrion (bottom) was imaged by SIM[51]. (f) TRPML1 activation preferentially increases mitochondrial calcium at mitochondria (red)-lysosome green contacts[101]. (g) The behavior of autophagy after the treatment of the antimicrobial drug (autophagy marker protein LC3 and p63)[97]. (h) Dual-color SIM images of dynamic physical interactions between lysosomes and mitochondria in live U2OS cells (Atto 647 N-magenta, Lysosome-565-green[99]. (i) Determination of co-localization of mitochondria with lysosomes after serum starvation[99].

could regulate the formation and unbinding of the MCS between lysosomes and mitochondria[39]. Autophagy is a protein-degrading behavior that efficiently removes long-lifetime and misfolded proteins, which contributes to maintaining cellular homeostasis[96]. Notably, lysosomes combine with intracellular autophagy ability to form autophagolysosomes, whose number, morphology, pH value, and distribution are related to tumorigenesis and progression[74,75]. Therefore, it is necessary to visualize and dynamically monitor the activity of autophagy-related proteins and their molecular mechanisms. Lumkwana *et al.*[97] visualized the correlation between the autophagy marker protein light chain 3 (LC3) and autophagy substrate (p63) with a resolution of 80 nm before and after treatment of antimicrobial drugs, as shown in Fig. 5(g). In addition, dSTORM with a resolution of 20 to 30 nm randomly alternated between light and dark to achieve the tracking and localization of p62, which provided a quantifiable method. Cisplatin has a good antitumor effect, but drug resistance reduces its effect during the treatment process. The reason for this is autophagy-enhanced MCS between mitochondria and lysosomes. Sheng *et al.*[98] found that cisplatin with a PI3K/mTOR inhibitor interfered with the mitochondria–lysosome interaction of liver cancer cells, which enhanced lysosomal membrane permeabilization, and drug resistance was relieved absolutely. The study of the interaction of organelles has guiding significance for the study of side effects of the chemotherapy effect. Han *et al.*[99] achieved real-time imaging for mitochondrial–lysozyme interaction during starvation therapy through SIM, whose spatial resolution and temporal resolution were 90 and 270, respectively, as illustrated in Figs. 5(h) and 5(i). More interestingly, it found that the behavior of autolysosomes was similar to lysosome behavior, which provides a new strategy for autophagy. Also, it has been discovered that mitochondrial–lysozyme interaction could regulate the progression of neurodegenerative diseases[100]. The activities of mitochondria and lysosomes are closely linked. The mitochondrial dysfunction leads to lysosomal damage due to increased reactive oxygen species, and dysfunctional lysosomes can also impair mitochondrial function.

3.2. The Interaction Effect between Mitochondria and Endoplasmic Reticulum

The endoplasmic reticulum (ER) is the largest organelle in the cell, the morphology of which is a network with a thickness of 5–6 nm. It is widely distributed in the cytoplasm and directly contacts the common intracellular membrane system to maintain the basic structure and function of the cell[89,102]. The spatial distribution of the endoplasmic reticulum was changed relatively by cellular fluidity, as depicted in Fig. 6(b)[89]. Among them, it communicates with mitochondria at a distance of 10 to 25 nm, which is suitable with fluorescence super-resolution technology. In addition, bioinformation such as ionic homeostasis, unfolded protein response (UPR), autophagy, and apoptosis is regulated by ER[103]. Compared with traditional light microscopes, FLSR could visualize the tightly packed diaphragm and tubular structures of ER. Schroeder *et al.*[104] realized dynamic substructural imaging in live cells by STED with a resolution of 50 nm and proved that its membrane contained a large number of small micropores synergistically regulated to tubules and cytoskeletons, as shown in Fig. 6(a). Man *et al.*[105] performed the chemical probe CLP-TMR combined with gene coding technology to detect the full width at half-maxima (FWHM), area, length, and number of nodes per unit area of ER in live cells by dSTORM, as shown in Fig. 6(c). In addition, temperature is an important factor for protein expression and cell activity, especially signaling pathways. Rodriguez-Gallardo *et al.*[106] used 3D super-resolution confocal live imaging microscopy (SCLIM) to compare and analyze the distribution of protein cargo in ER at different temperatures. The results clearly showed that protein cargo could easily penetrate the membrane of ER, which was distributed across membranes at medium temperature. The activity of protein cargo decreased at low temperatures.

As genetically characteristic organelles, mitochondrial DNA (mtDNA) regulates cellular-function-related RNA, protein transcription, and translation. On the one hand, the MCS between

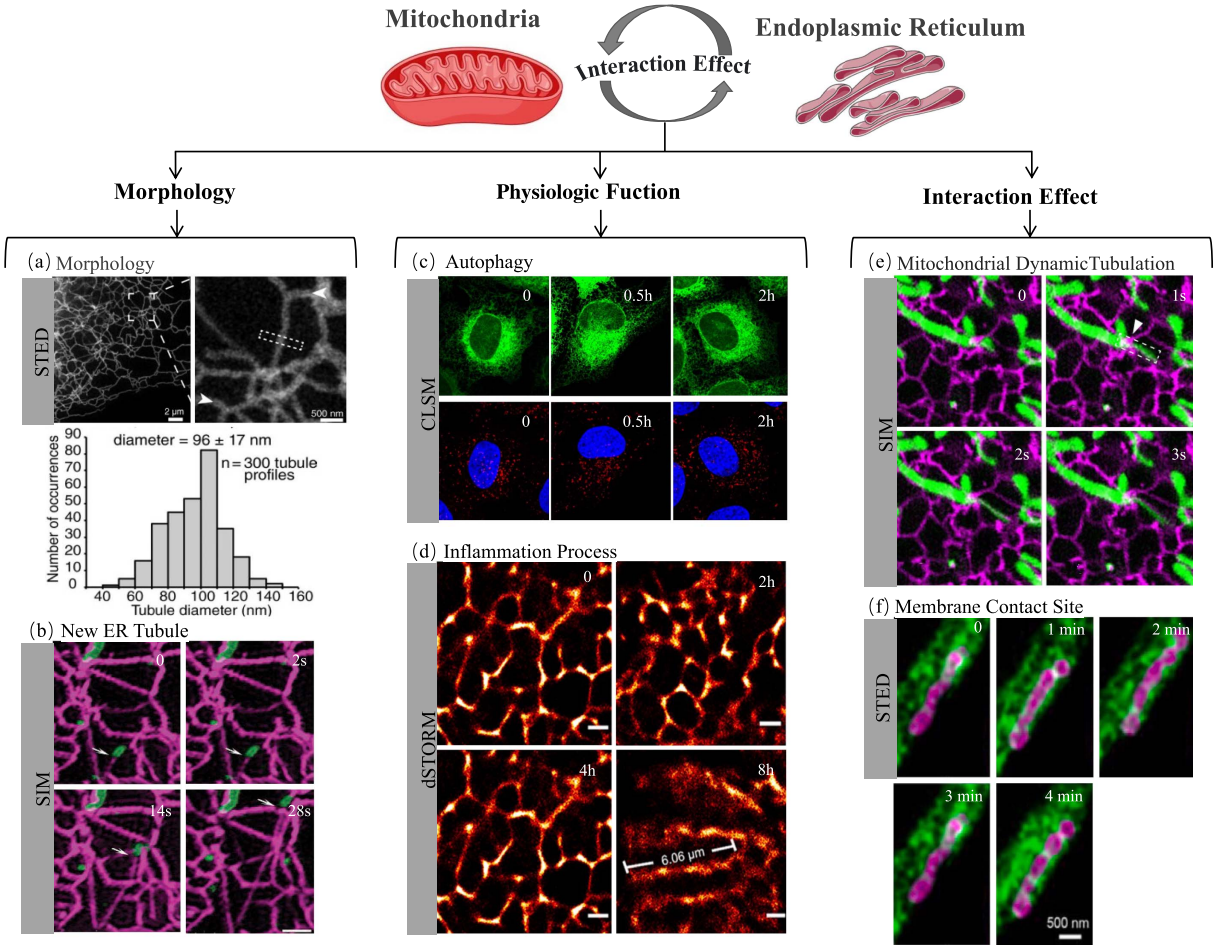

Fig. 6 The properties and interaction of mitochondria and endoplasmic reticulum. (a) The diameter of ER tubules labeled with SNAP-Sec61β was imaged. The spatial distribution of endoplasmic reticulum changes with the fluidity of live cells by STED[104]. (b) ER distribution changes during autophagy in U2OS cells[107]. (c) The morphological change of mitochondria during the process of autophagy[109]. (d) The morphological change of ER in live Hela cells was monitored by dSTORM under stress conditions[105]. (e) MDT at ER (magenta)–mitochondria (green) contacts were imaged by SIM[89]. (f) Two-color STED time-lapse imaging of ER-mitochondria interaction within a neurite[108].

ER and mitochondria, which is inherited by the next mitochondria, coordinates the synthesis and division of mtDNA. On the other hand, mitochondrial dynamic tubes promote the active transport of mtDNA. Qin *et al.*[89] performed real-time dynamic imaging of the mitochondrial dynamic tubulation (MDT) driven by KIF5B protein around the MCS by SIM, which verified the activity and transport mode of mtDNA, as presented in Fig. 6(d). In recent years, more and more studies have found that changes in structure and function around MCS play an important role in maintaining cell activity and the progression of disease. In addition, thinomycin antimicrobials mitigated the progression of inflammation by improving the area of the MCS[107]. The dynamic process of mitochondrial division and fusion is also closely related to the interaction effect of multiple organelles such as ER and lysosome. Boutry *et al.*[108] labeled vesicle-associated membrane proteins (VAPs) and lipid transfer protein ORP1L to test the three-way interaction effect between the ER, lysosome, and mitochondria, finding that the division of mitochondria was inhibited gradually. Guo *et al.*[109] used GI-SIM to monitor organelle interaction for a long time, whose temporal resolution and spatial resolution were 266 and 97 nm, respectively, confirming that MCS between ER and mitochondria promoted the growth of endoplasmic reticulum tubules and morphological changes in mitochondria, as shown in Fig. 6(f). Damenti *et al.*[110] used STED with a spatial resolution of 30 to 35 nm to track ER and mitochondria and found that the space of ER tubules was 120 to 500 nm apart, as depicted in Fig. 6(e). The ER tubules changed mitochondrial morphology, but mitochondrial deformation did not change the size of the ER. More interestingly, scholars also found that the size of the MCS was closely related to mitochondrial dynamics and local Ca^{2+} signaling, which can regulate the dynamics and structure of mitochondrial cristae membranes (CMs) to promote ionic balance between mitochondria and endoplasmic reticulum[111]. MCS between mitochondria and ER is involved in the replication and division of mitochondrial genetic material, which has broad implications for mechanisms of cell function, aging, and a range of diseases.

3.3. *The Interaction Effect between Mitochondria and Nucleus*

The nucleus consists of chromatin, RNA, nucleoli, and proteins, which is essential for genome folding and regulation. It is an important regulatory center for cytogenetics and metabolism[27]. The morphology of the nucleus is different, such as round or oval, with a diameter of 5 to 10 μm. As the most important organelle, nuclear pore complexes (NPCs) were fused by the inner and outer nuclear membranes to achieve the transmission of genetic material and information. With improved technology, STED could achieve super-resolution images for organelles, as illustrated in Fig. 7(f)[27]. Ma *et al.*[112] tracked the 3D spatial

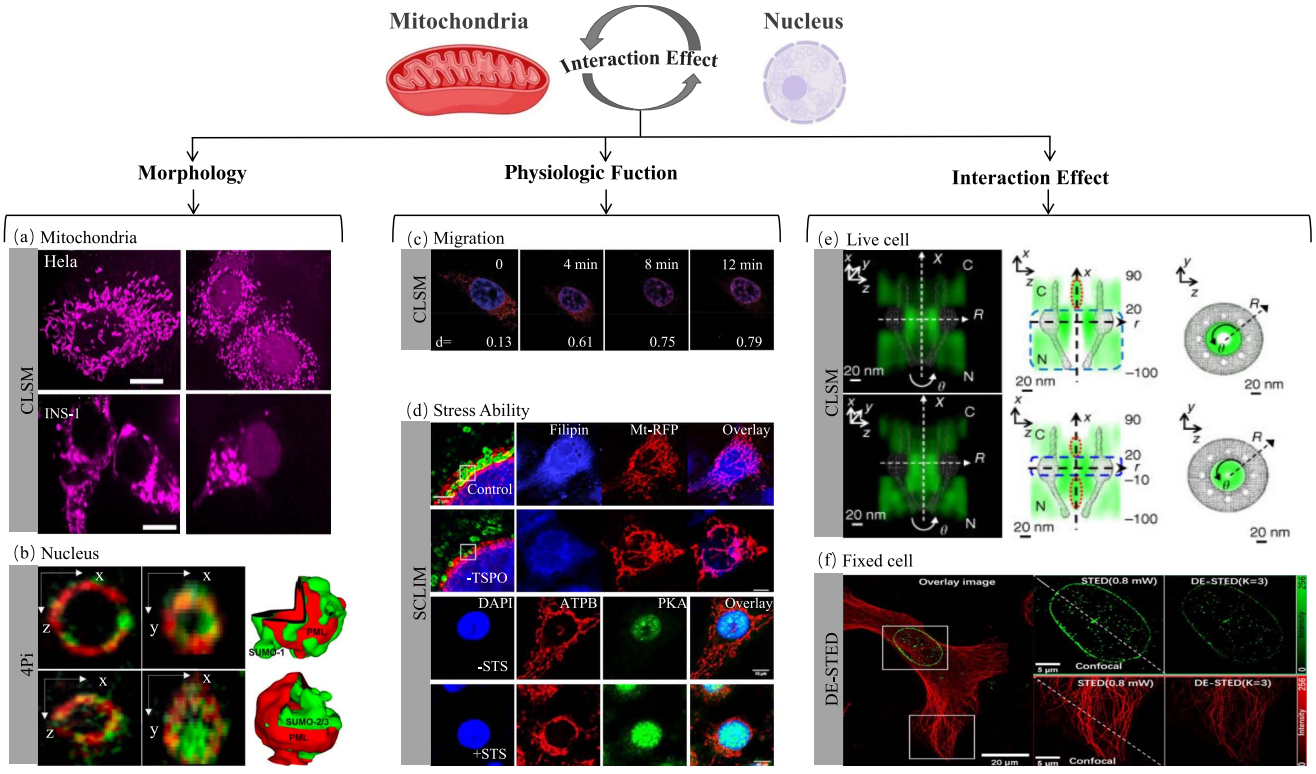

Fig. 7 The properties and interaction of the mitochondria and nucleus. (a) Representative confocal images of mito-STAR protein in HeLa and INS-1 cells[118]. (b) Two-color 4Pi microscopy images of PML and SUMO proteins[116]. (c) 3D tomography of interaction sites for Imp β1 in the NPCs (gray) of live cells[112]. (d) Dynamic tracking of the mitochondria (red)–nucleus (blue) migration via STED[120]. (e) TSPO regulates the stress ability of cells by changing the MCS between the mitochondria and nucleus[2]. (f) Two-color DE-STED imaging results from the same fixed U2OS cell including the nuclear membrane (green) and microtubules (red)[27].

distribution of passive transport through NPCs in live cells by single-point edge-excitation sub-diffraction (SPEED) and proposed that NPCs provided necessary competitive conditions for transportation, the results of which are shown in Fig. 7(c). The nucleus is located at the center of the cell, which requires higher-resolution techniques. The size of the NPCs is about 120 nm, but its internal structure is very fine. They can realize selective channel transmission of molecules of different properties and participate in multiple biological processes such as regulating the material exchange between the nucleus and the cytoplasm, gene expression, cellular signaling, and cell cycle. Gwosch *et al.*[113] conducted multicolor imaging and 3D reconstruction of the internal structure of fixed or living cells by MINFLUX. To demonstrate the differences in DNA structure, Eilers *et al.*[114] applied MINFLUX to the detection of rapid movements of a custom-designed DNA origami sample at different dimensions. Okada *et al.*[115] designed various fluorescent probes to compare differences in the nucleus and its internal structure by CLSM, SLM, and STED, in which STED obtained more precise nuclei structure. Chromatin is the core point of the nucleus and contains all human genetic information. Although the whole sequential genome has been detected, genetic regulation is still a challenge for biomedicine. Cremer *et al.*[116] designed spectral precision distance microscopy (SPDM) to achieve the visualization of genic regulation, which had the advantages of precise localization and quantitative analysis at the single-molecule level for the nucleus, such as in Fig. 7(b). The function of mitochondria is strictly regulated by nuclear activity, and their interaction plays a significant role in their function during the physiological and pathological progression. Eisenberg-Bord *et al.*[117] localized MCSs between mitochondria and organelles in yeast based on their membrane surface proteins, which provided channels for information exchange. The distribution of mitochondria in various cells is different. The density of the MCS between the mitochondria and nucleus in the cell membrane system is enhanced, and the morphology of mitochondria near the nucleus is easily observed during super-resolution imaging. Ramadani-Muja *et al.*[118] quantitatively analyzed subcellular localization and organelle distribution during the regulation of protein Sirt4 in stressful conditions, which mainly entered into the nucleus through the MCS, such as in Fig. 7(a). In addition, some scholars have found that the MCS promoted retrograde communication between mitochondria and the nucleus to improve cellular adaptation to stress, such as in Fig. 7(e)[119]. Xu *et al.*[120] designed aggregation-induced luminescence (AIEgen) with high photoluminescence quantum yield, good photostability, and biocompatibility, which achieved specific and dynamic imaging of subcellular structures for STED, as shown in Fig. 7(d). It increased the half-peak full width and imaging resolution during the migration processes of single nanoparticles. The interaction effect between mitochondria and the nucleus regulates the major epigenome and the mechanisms of the aging process, which promotes an understanding of interventions for human health and longevity.

3.4. The Interaction Effect between Endoplasmic Reticulum and Golgi Apparatus

As the last place for protein processing, the Golgi apparatus realizes the processing and packaging of proteins synthesized from ER. The morphology of the Golgi apparatus is usually arched or hemispherical with a thickness of 6 nm, which is composed of 3 to 7 flat vesicles with a diameter of 50 nm. Live cell fluorescence imaging puts forward higher requirements for the stability, phototoxicity, and photobleaching of dyes to maintain the normal activity and functional role of cells. Erdmann *et al.*[121] innovatively designed two photostable active dyes and compared the differences during dynamic processes of the Golgi apparatus in living cells by 3D confocal and STED, as shown in Fig. 8(a). The Trans-Golgi Network (TGN) is an important segment during the process of protein processing, classification, and transport, as depicted in Fig. 8(d)[122]. Shimizu *et al.*[123] designed a confocal microscopy technique with a multicolor and high spatiotemporal resolution for qualitative and quantitative analysis of the TGN in Arabidopsis thaliana herbaceous plants, and the TGN-related secretory transport and vacuole transport had different distribution and dynamic changes, as illustrated in Fig. 8(e). Zhang *et al.*[124] uses 4Pi single-molecule switch super-resolution microscopy with a resolution of 5 to 10 nm to accurately locate flat vesicle matrices and transporters in the Golgi apparatus, which can realize efficient analysis for the Golgi curled structure and MCS, as presented in Fig. 8(b). Some research verified that methionine sulfoxide oxidase was related to the tube bubble structure and exhibited significant co-determination with markers of the Golgi apparatus and circulating endosomes. Sikora *et al.*[125] observed a high correlation distribution of GM130 and MICAL-L1 around the nucleus by confocal imaging, which was precisely located at different Golgi cisternae by STORM, as shown in Fig. 8(c). Herrera *et al.*[126] achieved located imaging for reverse transport of bacterial toxins around TGN by STED, such as ricin and cholera toxin.

3.5. The Interaction Effect between Membraneless Organelles

The cells maintain their normal structure and function through the cell membrane system for material exchange and information communication. The centrosome is distributed in the cell matrix near the nucleus and consists of two mutually perpendicular centrioles, while the diameter and length are 0.16 to 0.23 μm and 0.16 to 0.56 μm, respectively, the results of which are shown in Fig. 9(d)[127]. It is important for centrosomes to regulate cell activity and organelle interaction effects. It is the center of the microtubule that plays a regulatory role in maintaining the number, stability, and spatial distribution of microtubules. The shape of the distal centriole assembly (DAP) is described as a pinwheel. Yang *et al.*[128] redefined the pinwheel as a cone-shaped structure by dSTORM with a frequency of 50 frame/s as shown in Fig. 9(b). Sydor *et al.*[129] found the PPP1R35 widely was distributed in the proximal lumen of the centrosome, which co-work with RTTN to affect the number of centrosomes and the structure of centrioles. Expansion microscopy (ExM) was first proposed by Ed Boyden in 2015. Its resolution can reach 70 nm under a typical expansion of about four times based on the traditional confocal microscope[130]. Zwettler *et al.*[131] combined dSTORM with ExM to improve imaging resolution to 20 nm, the result of which enhanced the ultrastructural imaging and labeling rate of microtubules and centrioles, as depicted in Fig. 9(e). As an intracellular membraneless organelle, the ribosome, mainly composed of protein and RNA, is the place for intracellular protein synthesis. Ribosomes are ellipsoidal granular bodies with a diameter of 20–30 nm. It can be divided into a 60 S large subunit and

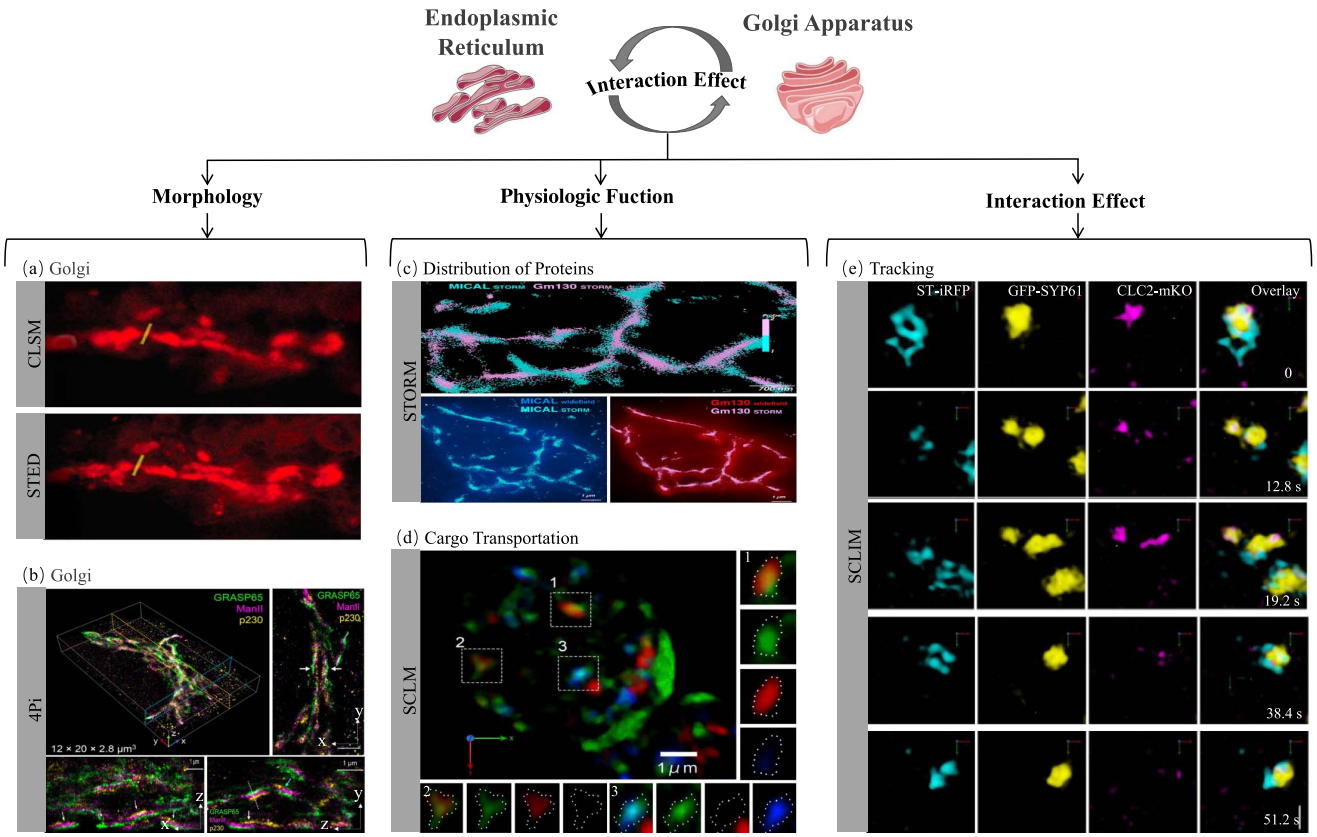

Fig. 8 The properties and interaction of the endoplasmic reticulum and Golgi apparatus. (a) Confocal and STED images of the Golgi[121]. (b) Complex stacked architecture of the Golgi apparatus by the 4Pi single-molecule switched super-resolution microscope[91]. (c) The distribution of MICAL-L1/TGN46, MICAL-L1/ GM130, and MICAL-L1/TfR colocalization was evaluated by STORM[125]. (d) Cargo (green) is transported from cis-Golgi (red) to TGN (blue) while being maintained in a maturing cisterna[122]. (e) 4D images of the Golgi apparatus, TGN, and secretory trafficking zone component clathrin in the epidermal cell of the root elongation zone under SCLIM[125].

a 40 S small subunit according to the sedimentation coefficient. Ruland *et al.*[132] combined single-molecule tracking and super-resolution confocal microscopy with an imaging time of 24 ms to realize the intracellular transport kinetics of the ribosome large subunit structure in the NPC, the results of which are shown in Fig. 9(c). Deng *et al.*[133] conducted single-molecule activity and real-time dynamic localization of the ribosome substructure and its cell–matrix interaction effects in motor neuron injury diseases by STORM, whose numerical aperture (NA) was 1.49. It further showed that neurological dysfunction changed the subcellular structure of ribosome and axonal ER interaction effector responses. Ribosomes are responsible for completing the "translation" process from RNA to protein in the "central dogma" in cells. Simply, the small subunit of the ribosome before translation is combined with the messenger RNA (mRNA) transcribed from the nucleus and then met with the large subunit to form a complete ribosome. Polypeptides were synthesized through the transfer RNA (tRNA) in the cytoplasmic matrix, which is the first key step in the ribosome synthesis of proteins. Maiser *et al.*[134] analyzed the spatial fluorescence distribution of the transcribed gene rDNA by 3D-SIM. That was inconsistent with the spatial distribution of rRNA, which makes up for the corresponding spatial proteomics, as illustrated in Fig. 9(a).

Super-resolution imaging techniques enable localization and tracking of proteins at the subcellular level by breaking through the diffraction limit. And biologists are trying to improve sample quality from the sample labeling techniques and dye upgrade, for example, the combination of 3D super-resolution and block-face electron microscopy, PAINT techniques, and expansion techniques breaks. Hoffman *et al.*[135] developed a platform for 3D cryogenic super-resolution imaging and focused ion-beam-milled block-face EM across entire vitreously frozen cells with an accuracy of 40 nm. This technique could achieve super-resolution imaging for endoplasmic reticulum, peroxisomes, and neurons, which elucidated these details by directly visualizing the nanoscale relationship of specific proteins in the context of the global cellular ultrastructure. Klimas *et al.*[136] used a mechanically sturdy gel that retains nucleic acids, proteins, and lipids without the need for a separate anchoring step, and the sturdy gel could magnify the cell-specific markers. The resolution was increased to 15 nm, which was suitable for subcellular structures. In response to fluorescence artifacts caused by chemical fixation, Laporte *et al.*[137] used a combination of cryofixation and expansion microscopy (Cryo-ExM) to preserve the native cellular state. The fluorescent labeling size of traditional primary and secondary antibodies is 15 to 20 nm, while the interaction effect of a single biomolecule is generally below

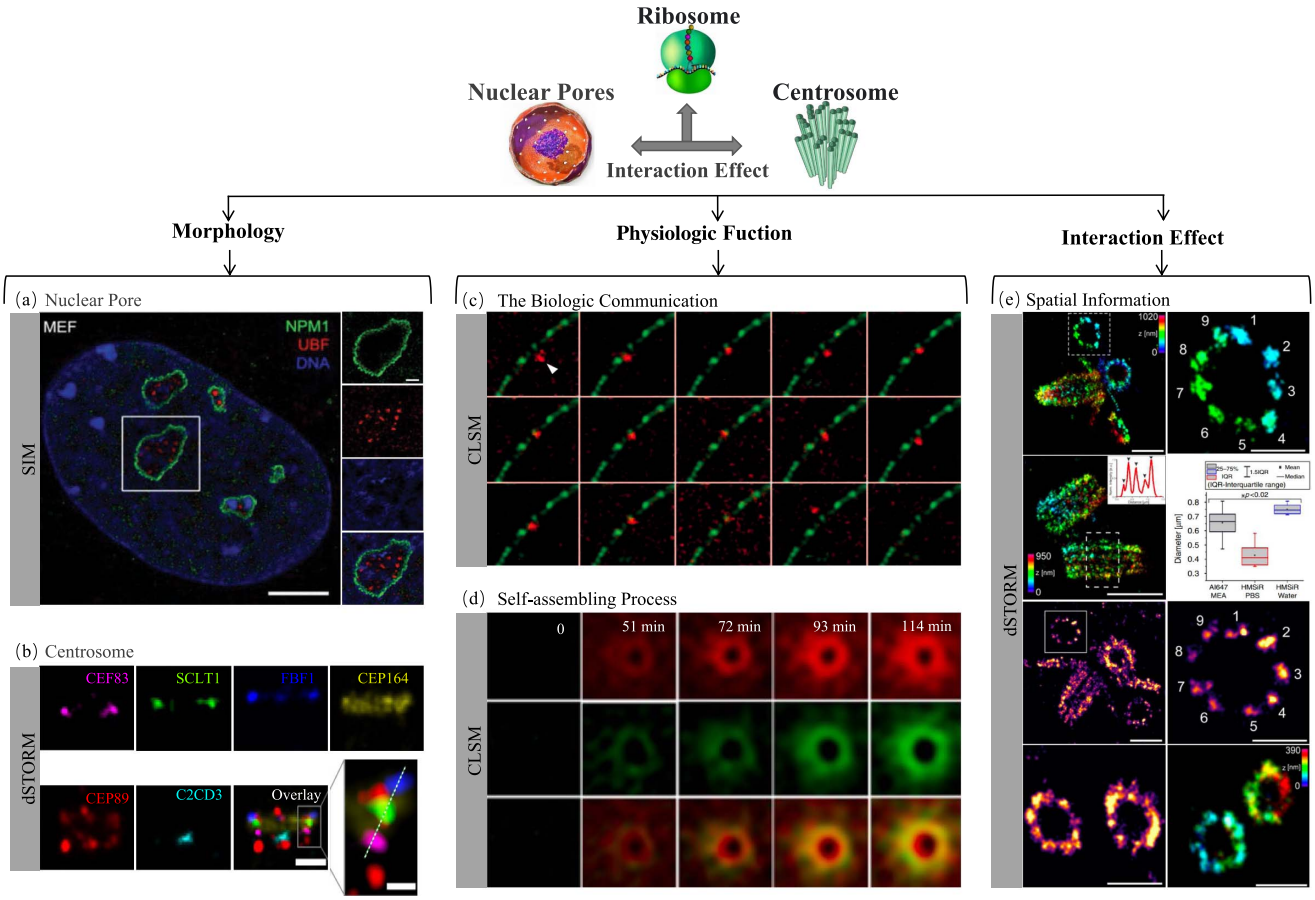

Fig. 9 The properties and interaction of membraneless organelles. (a) Super-resolution 3D-SIM imaging of nucleolar organization[134]. (b) The super-resolution imaging of centriole distal by dual-channel dSTORM[128]. (c) The biological communication of the cytoplasm by the NPC[132]. (d) SIM-TIRF time-lapse of the self-assembling process of the centrosome *in vitro*[127]. (e) 3D and 2D dSTORM images of U-ExM expanded and re-embedded chlamydomonas centrioles[127].

10 nm. So it is necessary to improve the resolution of super-resolution imaging techniques. Reinhardt *et al.*[138] used effectively acquired localization of the single protein molecules CD20 by sequential imaging (RESI) techniques.

It is essential for the quality of the fluorescence super-resolution image to choose the optimal performance and size of dyes. The brightness and stability are necessary for STED and SIM, especially for the real-time imaging of live cells. In addition, the fluorophore should also have reversible scintillation characteristics for SMLM techniques. Specific targeting groups are targeted by small molecule dyes during labeling of different organelles. Mitochondria, an energy source for cellular activities, has complicated and diverse structures and functions. According to its potential and lipid solubility, IMMBright660, MitoPB Yellow, mtDNA, and SYBRTMGold were designed to achieve super-resolution imaging of mitochondrial membranes, internal cristae, mitochondrial matrix, and DNA. With the maturity of super-resolution fluorescence imaging techniques, the development of fluorochromes has acquired new opportunities and challenges at the beginning of the 21st century. The next generation of fluorescent dyes will focus on dye performance, super-resolution fluorescence imaging resolution, multi-imaging mode fusion, and multi-level targeted labeling to drive new breakthroughs in basic research involved in cell biology and medicine.

4. Conclusion and Outlook

Methodologically, super-resolution microscopy technology had excellent high-resolution superiorities compared with other fluorescent technologies represented by confocal imaging techniques, which have been widely applied in the field of life sciences. In this review, we have declared the original principles and developments of the FLSR technique. Based on each characteristic, more details of biomedical sciences have been found gradually. This not only acquires a large field of view of the morphology and spatial distribution of biological molecules but also obtains three-dimensional interaction effects of different organelles such as mitochondria and lysosomes during cell dynamic processes. The super-resolution technologies provide accurate analysis for physiological and pathological problems, which have great potential for biomedical applications during the process of precision medicine.

In the past two decades, technological innovation has led to the development of a still-growing number of useful super-resolution microscopy methods that are able to fulfill many of the requirements for detailed analysis of basic biology on the

nanoscale. The imaging system may be further optimized with increasing application. Since the reconstruction process requires a mass of samples and time, it decreases its real-time analysis capabilities. For example, the image processing method based on deep learning can shorten the super-resolution imaging time to a certain extent. The optimization and update of the algorithm are feasible means. Multi-modal imaging analysis can combine the advantages of various technologies at the maximum, the results of which will improve the sensitivity of super-resolution technology. The good biosafety of fluorescence should be considered indispensably *in vivo*, so fluorescent probes or dyes can ensure high-resolution imaging while reducing their ability to damage cells, such as phototoxicity and photobleaching. Overall, the performance of various super-resolution imaging technologies could be improved by algorithms, hardware platforms, and fluorescent probes, which will discover more breakthroughs and medical applications for scientists. That novel perspective may monitor a series of dynamic processes comprehensively represented by extracellular or intracellular interaction, nanoparticle tracking, disease progression, and nanomedicine or nano-investigations in the future.

Acknowledgments

This work was supported by the National Natural Science Foundation of China (Nos. 62275125 and 62227818) and the Fundamental Research Funds for the Central Universities (Nos. 30922010313 and 30924010913).

References

1. A. Calcinotto *et al.*, "Cellular senescence: aging, cancer, and injury," *Physiol. Rev.* **99**, 1047 (2019).
2. M. Picard and O S. Shirihai, "Mitochondrial signal transduction," *Cell Metab.* **34**, 1620 (2022).
3. D. B. Zorov, M. Juhaszova, and S. J. Sollott, "Mitochondrial reactive oxygen species (ROS) and ROS-induced ROS release," *Physiol. Rev.* **94**, 909 (2014).
4. D. M. Pegtel and S. J. Gould, "Exosomes," *Annu. Rev. Biochem.* **88**, 487 (2019).
5. I. Rodriguez-Hernandez *et al.*, "WNT11-FZD7-DAAM1 signalling supports tumour initiating abilities and melanoma amoeboid invasion," *Nat. Commun.* **11**, 5315 (2020).
6. Y. Cheng *et al.*, "Targeting CXCR2 inhibits the progression of lung cancer and promotes therapeutic effect of cisplatin," *Mol. Cancer* **20**, 62 (2021).
7. D. Bhattacharya, O. Oresajo, and A. Scimè, "p107 mediated mitochondrial function controls muscle stem cell proliferative fates," *Nat. Commun.* **12**, 5977 (2021).
8. R. Han *et al.*, "Recent advances in super-resolution fluorescence imaging and its applications in biology," *J. Genet. Genomics* **40**, 583 (2013).
9. M. J. Rust, M. Bates, and X. Zhuang, "Sub-diffraction-limit imaging by stochastic optical reconstruction microscopy (STORM)," *Nat. Methods* **3**, 793 (2006).
10. J. Xu, K. F. Tehrani, and P. Kner, "Multicolor 3D super-resolution imaging by quantum dot stochastic optical reconstruction microscopy," *ACS Nano* **9**, 2917 (2015).
11. M. Bates *et al.*, "Optimal precision and accuracy in 4Pi-STORM using dynamic spline PSF models," *Nat. Methods* **19**, 603 (2022).
12. H. Blom and J. Widengren, "Stimulated emission depletion microscopy," *Chem. Rev.* **117**, 7377 (2017).
13. P. N. Hedde *et al.*, "Stimulated emission depletion-based raster image correlation spectroscopy reveals biomolecular dynamics in live cells," *Nat. Commun.* **4**, 2093 (2013).
14. D. Li *et al.*, "Extended-resolution structured illumination imaging of endocytic and cytoskeletal dynamics," *Science* **349**, 3500 (2015).
15. M. G. L. Gustafsson *et al.*, "Three-dimensional resolution doubling in wide-field fluorescence microscopy by structured illumination," *Biophys. J.* **94**, 4957 (2008).
16. F. Balzarotti *et al.*, "Nanometer resolution imaging and tracking of fluorescent molecules with minimal photon fluxes," *Science* **355**, 606 (2017).
17. R. Schmidt *et al.*, "MINFLUX nanometer-scale 3D imaging and microsecond-range tracking on a common fluorescence microscope," *Nat. Commun.* **12**, 1478 (2021).
18. J. K. Pape, *et al.*, "Multicolor 3D MINFLUX nanoscopy of mitochondrial MICOS proteins," *Proc. Natl. Acad. Sci. U.S.A.* **117**, 20607 (2020).
19. E. Betzig *et al.*, "Imaging intracellular fluorescent proteins at nanometer resolution," *Science* **313**, 1642 (2006).
20. M. Heilemann *et al.*, "Subdiffraction resolution fluorescence imaging with conventional fluorescent probes," *Angewandte Chemie* **47**, 6172 (2008).
21. B. Huang *et al.*, "Three-dimensional super-resolution imaging by stochastic optical reconstruction microscopy," *Science* **319**, 810 (2008).
22. L. Zhu *et al.*, "Faster STORM using compressed sensing," *Nat. Methods* **9**, 721 (2012).
23. S. A. Jones *et al.*, "Fast, three-dimensional super-resolution imaging of live cells," *Nat. Methods* **8**, 499 (2011).
24. W. Ouyang *et al.*, "Deep learning massively accelerates super-resolution localization microscopy," *Nat. Biotechnol.* **36**, 460 (2018).
25. A. Ghosh *et al.*, "Graphene- and metal-induced energy transfer for single-molecule imaging and live-cell nanoscopy with (sub)-nanometer axial resolution," *Nat. Protoc.* **16**, 3695 (2021).
26. M. Weber *et al.*, "MINSTED fluorescence localization and nanoscopy," *Nat. Photonics* **15**, 361 (2021).
27. J. Zhang *et al.*, "Low-power two-color stimulated emission depletion microscopy for live cell imaging," *Biosensors* **11**, 330 (2021).
28. Y. Liu *et al.*, "Population control of upconversion energy transfer for stimulation emission depletion nanoscopy," *Adv. Sci.* **10**, 2205990 (2023).
29. A. Benda *et al.*, "STED imaging of tau filaments in Alzheimer's disease cortical grey matter," *J. Struct. Biol.* **195**, 345 (2016).
30. T. J. Gould *et al.*, "Adaptive optics enables 3D STED microscopy in aberrating specimens," *Opt. Express* **20**, 20998 (2012).
31. P. Zdankowski *et al.*, "Numerically enhanced stimulated emission depletion microscopy with adaptive optics for deep-tissue super-resolved imaging," *ACS Nano* **14**, 394 (2019).
32. L. Wang *et al.*, "Low-power STED nanoscopy based on temporal and spatial modulation," *Nano Res.* **15**, 3479 (2022).
33. B. R. Patton *et al.*, "Three-dimensional STED microscopy of aberrating tissue using dual adaptive optics," *Opt. Express* **24**, 8862 (2016).
34. P. Gao *et al.*, "Background suppression in fluorescence nanoscopy with stimulated emission double depletion," *Nat. Photonics* **11**, 163 (2017).
35. C. Kuang *et al.*, "Breaking the diffraction barrier using fluorescence emission difference microscopy," *Sci. Rep.* **3**, 1441 (2013).
36. Y. Liu *et al.*, "Super-resolution mapping of single nanoparticles inside tumor spheroids," *Small* **16**, e1905572 (2020).
37. Y. Liu *et al.*, "On-chip mirror enhanced multiphoton upconversion super-resolution microscopy," *Nano Lett.* **23**, 5514 (2023).
38. C. Chen *et al.*, "Multi-photon near-infrared emission saturation nanoscopy using upconversion nanoparticles," *Nat. Commun.* **9**, 3290 (2018).
39. J. Wang *et al.*, "Improving the image quality in STED nanoscopy using frequency spectrum modulation," *J. Biophotonics* **14**, e202000402 (2021).

40. W. I. Zhang *et al.*, "Fluorescent in situ hybridization of synaptic proteins imaged with super-resolution STED microscopy," *Microsc. Res. Tech.* **77**, 517 (2014).
41. J. G. Schloetel *et al.*, "Guided STED nanoscopy enables super-resolution imaging of blood stage malaria parasites," *Sci. Rep.* **9**, 4674 (2019).
42. L. Wang *et al.*, "Ultralow power demand in fluorescence nanoscopy with digitally enhanced stimulated emission depletion," *Nanophotonics* **9**, 831 (2020).
43. R. Fukaya *et al.*, "Increased vesicle fusion competence underlies long-term potentiation at hippocampal mossy fiber synapses," *Sci. Adv.* **9**, 3616 (2023).
44. M. G. M. Velasco *et al.*, "3D super-resolution deep-tissue imaging in living mice," *Optica* **8**, 442 (2021).
45. L. Finzel and M. Reuss, "A stimulated emission depletion (STED) microscope of all trades," *IMicroscopy Today* **30**, 26 (2022).
46. J. Bucevičius *et al.*, "A general highly efficient synthesis of biocompatible rhodamine dyes and probes for live-cell multicolor nanoscopy," *Nat. Commun.* **14**, 1306 (2023).
47. M. G. L. Gustafsson, "Surpassing the lateral resolution limit by a factor of two using structured illumination microscopy," *J. Microsc.* **198**, 82 (2000).
48. C. Eggeling *et al.*, "Lens-based fluorescence nanoscopy," *Q. Rev. Biophys.* **48**, 178 (2015).
49. L. Shao *et al.*, "Super-resolution 3D microscopy of live whole cells using structured illumination," *Nat. Methods* **8**, 1044 (2011).
50. P. Kner *et al.*, "Super-resolution video microscopy of live cells by structured illumination," *Nat. Methods* **6**, 339 (2009).
51. X. Huang *et al.*, "Fast, long-term, super-resolution imaging with Hessian structured illumination microscopy," *Nat. Biotechnol.* **36**, 451 (2018).
52. Mgl Gustafsson, "Nonlinear structured-illumination microscopy: wide-field fluorescence imaging with theoretically unlimited resolution," *Proc. Natl. Acad. Sci. U.S.A.* **102**, 13081 (2005).
53. E. Hesper Rego *et al.*, "Nonlinear structured-illumination microscopy with a photoswitchable protein reveals cellular structures at 50-nm resolution," *Proc. Natl. Acad. Sci. U.S.A.* **109**, 661 (2012).
54. L. Shao *et al.*, "I5S: wide-field light microscopy with 100-nm-scale resolution in three dimensions," *Biophys J.* **94**, 4971 (2008).
55. L. A. Masullo *et al.*, "Pulsed interleaved MINFLUX," *Nano Lett.* **21**, 840 (2020).
56. T. Schlichthaerle, C. Lindner, and R. Jungmann, "Super-resolved visualization of single DNA-based tension sensors in cell adhesion," *Nat. Commun.* **12**, 2510 (2021).
57. D. J. Williamson, *et al.*, "Multi-color molecular visualization of signaling proteins reveals how c-terminal Src kinase nanoclusters regulate T cell receptor activation," *Cell Rep.* **33**, 108523 (2020).
58. C. Niederauer *et al.*, "Dual-color DNA-paint single-particle tracking enables extended studies of membrane protein interactions," *Nat. Commun.* **14**, 4345 (2023).
59. J. Zähringer *et al.*, "Combining pMINFLUX, graphene energy transfer and DNA-PAINT for nanometer precise 3D super-resolution microscopy," *Light Sci. Appl.* **12**, 70 (2023).
60. L. A. Masullo *et al.*, "An alternative to MINFLUX that enables nanometer resolution in a confocal microscope," *Light Sci. Appl.* **11**, 199 (2022).
61. L. M. Ostersehlt *et al.*, "DNA-PAINT MINFLUX nanoscopy," *Nat. Methods* **19**, 1072 (2022).
62. K. Zhao *et al.*, "Two-photon MINFLUX with doubled localization precision," *eLight* **2**, 5 (2022).
63. A. J. Graham, M. T. Robinson, and A. Z. Maleki, "Rapid on-site evaluation (ROSE) of image-guided FNA specimens improves subsequent core biopsy adequacy in clinical trial patients: The impact of preanalytical factors and its correlation with survival," *Cancer Cytopathol.* **132**, 30 (2024).
64. V. Ebrahimi *et al.*, "Deep learning enables fast, gentle STED microscopy," *Commun. Biol.* **6**, 674 (2023).
65. X. Chen *et al.*, "Gated-GAN: adversarial gated networks for multi-collection style transfer," *IEEE Trans. Image Process.* **28**, 546 (2018).
66. H. Wu, *et al.*, "Localizing axial dense emitters based on single-helix point spread function and deep learning," arXiv:2407.07681 (2024).
67. E. Nehme *et al.*, "Deep-storm: super-resolution single-molecule microscopy by deep learning," *Optica* **5**, 458 (2018).
68. J. Li *et al.*, "Spatial and temporal super-resolution for fluorescence microscopy by a recurrent neural network," *Opt. Express* **29**, 15747 (2021).
69. A. Speiser *et al.*, "Deep learning enables fast and dense single-molecule localization with high accuracy," *Nat. Methods* **18**, 1082 (2021).
70. Z. H. Shah *et al.*, "Deep-learning based denoising and reconstruction of super-resolution structured illumination microscopy images," *Photonics Res.* **9**, B168 (2021).
71. Y. Chen *et al.*, "Deep learning enables contrast-robust super-resolution reconstruction in structured illumination microscopy," *Opt. Express* **32**, 3316 (2024).
72. M. A. Boland *et al.*, "Improving axial resolution in structured illumination microscopy using deep learning," *Philos. Trans. R. Soc. A* **379**, 20200298 (2021).
73. S. M. Davidson *et al.*, "Direct evidence for cancer-cell-autonomous extracellular protein catabolism in pancreatic tumors," *Nat. Med.* **23**, 235 (2016).
74. S. Zhu *et al.*, "Lysosomal quality control of cell fate: a novel therapeutic target for human diseases," *Cell Death Dis.* **11**, 817 (2020).
75. L. Xu *et al.*, "Downregulation of α-$_L$-fucosidase 1 suppresses glioma progression by enhancing autophagy and inhibiting macrophage infiltration," *Cancer Sci.* **111**, 2284 (2020).
76. H. Kim *et al.*, "Structural basis for mitoguardin-2 mediated lipid transport at ER-mitochondrial membrane contact sites," *Nat. Commun.* **13**, 3702 (2022).
77. A. Paden King and J. J. Wilson, "Endoplasmic reticulum stress: an arising target for metal-based anticancer agents," *Nat. Commun.* **49**, 8113 (2022).
78. J. Wang, Y. Wang, and W. Liang, "Delivery of drugs to cell membranes by encapsulation in PEG-PE micelles," *J. Control Release* **160**, 637 (2012).
79. S. Pollock *et al.*, "Uptake and trafficking of liposomes to the endoplasmic reticulum," *FASEB J.* **24**, 1866 (2010).
80. T. Wang *et al.*, "Cellular uptake of nanoparticles by membrane penetration: a study combining confocal microscopy with FTIR spectroelectrochemistry," *ACS Nano* **6**, 1251 (2012).
81. R. Y. Yu *et al.*, "Regulating Golgi apparatus by co-delivery of COX-2 inhibitor and brefeldin a for suppression of tumor metastasis," *Biomater. Sci.* **6**, 2144 (2018).
82. M. Misuth *et al.*, "The flashlights on a distinct role of protein kinase C: phosphorylation of regulatory and catalytic domain upon oxidative stress in glioma cells," *Cell. Signal.* **34**, 11 (2017).
83. C. M. Deus *et al.*, "Mitochondria-lysosome crosstalk: from physiology to neurodegeneration," *Trends Mol. Med.* **26**, 71 (2020).
84. N. Dahan *et al.*, "Peroxisome function relies on organelle-associated mRNA translation," *Sci. Adv.* **8**, eabk2141 (2022).
85. N. Mizushima *et al.*, "Autophagy fights disease through cellular self-digestion," *Nature* **451**, 1069 (2008).
86. D. D. Newmeyer and S. Ferguson-Miller, "Mitochondria: releasing power for life and unleashing the machineries of death," *Cell* **112**, 481 (2003).
87. E. Betzig *et al.*, "Imaging intracellular fluorescent proteins at nanometer resolution," *Science* **313**, 1642 (2006).

88. C. Wang *et al.*, "Dynamic tubulation of mitochondria drives mitochondrial network formation," *Cell Res.* **25**, 1108 (2015).
89. J. Qin *et al.*, "ER-mitochondria contacts promote mtDNA nucleoids active transportation via mitochondrial dynamic tabulation," *Nat. Commun.* **11**, 4471 (2020).
90. B. Chen *et al.*, "STORM imaging of mitochondrial dynamics using a vicinal-dithiol-proteins-targeted probe," *Biomaterials* **243**, 119938 (2020).
91. C. A. Wurm *et al.*, "Nanoscale distribution of mitochondrial import receptor Tom20 is adjusted to cellular conditions and exhibits an inner-cellular gradient," *Proc. Natl. Acad. Sci. U.S.A.* **108**, 13546 (2021).
92. G. Donnert *et al.*, "Two-color far-field fluorescence nanoscopy," *Biophys. J.* **92**, L67 (2007).
93. R. Schmidt *et al.*, "Mitochondrial cristae revealed with focused light," *Nano Lett.* **9**, 2508 (2009).
94. H. Fang and J. Diao, "*De Novo*-designed near-infrared nanoaggregates for the superresolution monitoring of lysosomes in cells, in whole organoids, and *in vivo*," *Biophys. J.* **118**, 2656 (2020).
95. Y. C. Wong, W. Peng, and D. Krainc, "Lysosomal regulation of inter-mitochondrial contact fate and motility in Charcot-Marie-Tooth type 2," *Dev. Cell* **50**, 339 (2019).
96. N. Mizushima and M. Komatsu, "Autophagy: renovation of cells and tissues," *Cell* **147**, 728 (2011).
97. D. Lumkwana, L. Engelbrecht, and B. Loos, "Monitoring autophagy using super-resolution structured illumination and direct stochastic optical reconstruction microscopy," *Methods Cell Biol.* **165**, 139 (2021).
98. J. Sheng *et al.*, "Inhibition of PI3K/mTOR increased the sensitivity of hepatocellular carcinoma cells to cisplatin via interference with mitochondrial-lysosomal crosstalk," *Cell Prolif.* **52**, 12609 (2019).
99. Y. Han *et al.*, "Cell-permeable organic fluorescent probes for live-cell long-term super-resolution imaging reveal lysosome-mitochondrion interactions," *Nat. Commun.* **8**, 1307 (2017).
100. D. Valdinocci *et al.*, "Alpha-synuclein aggregates associated with mitochondria in tunnelling nanotubes," *Neurotoxic. Res.* **39**, 429 (2021).
101. W. Peng, Y. C. Wong, and D. Krainc, "Mitochondria-lysosome contacts regulate mitochondrial Ca^{2+} dynamics via lysosomal TRPML1," *Proc. Natl. Acad. Sci. U S A* **117**, 19266 (2020).
102. V. Allan, "Intertwined and finely balanced: endoplasmic reticulum morphology, dynamics, function, and diseases," *Cells* **10**, 2341 (2021).
103. X. Chen and J. R. Cubillos-Ruiz, "Endoplasmic reticulum stress signals in the tumour and its microenvironment," *Nat. Rev. Cancer* **21**, 71 (2020).
104. L. K. Schroeder *et al.*, "Dynamic nanoscale morphology of the ER surveyed by STED microscopy," *J. Cell Biol.* **218**, 83 (2019).
105. H. Man *et al.*, "Hybrid labeling system for dSTORM imaging of endoplasmic reticulum for uncovering ultrastructural transformations under stress conditions," *Biosens. Bioelectron.* **189**, 113378 (2021).
106. S. Rodriguez-Gallardo *et al.*, "Assay for dual cargo sorting into endoplasmic reticulum exit sites imaged by 3D super-resolution confocal live imaging microscopy (SCLIM)," *PloS One* **16**, e0258111 (2021).
107. A. Filipe *et al.*, "Defective endoplasmic reticulum-mitochondria contacts and bioenergetics in SEPN1-related myopathy," *Cell Death Differ.* **28**, 123 (2020).
108. M. Boutry and P. K. Kim, "ORP1L mediated PI(4)P signaling at ER-lysosome-mitochondrion three-way contact contributes to mitochondrial division," *Nat. Commun.* **12**, 5354 (2021).
109. Y. Guo *et al.*, "Visualizing intracellular organelle and cytoskeletal interactions at nanoscale resolution on millisecond timescales," *Cell* **175**, 1430 (2018).
110. M. Damenti *et al.*, "STED and parallelized RESOLFT optical nanoscopy of the tubular endoplasmic reticulum and its mitochondrial contacts in neuronal cells," *Neurobiol Dis.* **155**, 105361 (2021).
111. B. Gottschalk *et al.*, "Intracellular Ca^{2+} release decelerates mitochondrial cristae dynamics within the junctions to the endoplasmic reticulum," *Pfluegers Arch.* **470**, 1193 (2018).
112. J. Ma, A. Goryaynov, and W. Yang, "Super-resolution 3D tomography of interactions and competition in the nuclear pore complex," *Nat. Struct. Mol. Biol.* **23**, 239 (2016).
113. K. C. Gwosch *et al.*, "MINFLUX nanoscopy delivers 3D multicolor nanometer resolution in cells," *Nat. Methods* **17**, 217 (2020).
114. Y. Eilers *et al.*, "MINFLUX monitors rapid molecular jumps with superior spatiotemporal resolution," *Proc. Natl. Acad. Sci. U S A* **115**, 6117 (2018).
115. Y. Okada and S. Nakagawa, "Super-resolution imaging of nuclear bodies by STED microscopy," in *Super-Resolution Imaging of Nuclear Bodies by STED Microscopy*, Vol. **1262** (Humana Press, 2015), p. 21.
116. C. Cremer *et al.*, "Super-resolution microscopy approaches to nuclear nanostructure imaging," *Methods* **123**, 11 (2017).
117. M. Eisenberg-Bord *et al.*, "Cnm1 mediates nucleus–mitochondria contact site formation in response to phospholipid levels," *J. Cell Biol.* **220**, e202104100 (2021).
118. J. Ramadani-Muja *et al.*, "Visualization of Sirtuin 4 distribution between mitochondria and the nucleus, based on bimolecular fluorescence self-complementation," *Cells* **8**, 1583 (2019).
119. R. Desai, *et al.*, "Mitochondria form contact sites with the nucleus to couple pro-survival retrograde response," *Sci. Adv.* **6**, eabc9955 (2020).
120. Y. Xu *et al.*, "Aggregation-induced emission (AIE) in super-resolution imaging: cationic AIE luminogens (AIEgens) for tunable organelle-specific imaging and dynamic tracking in nanometer scale," *ACS Nano* **16**, 1583 (2022).
121. R. S. Erdmann *et al.*, "Super-resolution imaging of the Golgi in live cells with a bioorthogonal ceramide probe," *Angewandte Chemie* **53**, 10242 (2014).
122. K. Kurokawa *et al.*, "Visualization of secretory cargo transport within the Golgi apparatus," *J Cell Biol.* **218**, 1602 (2019).
123. Y. Shimizu *et al.*, "Cargo sorting zones in the trans-Golgi network visualized by super-resolution confocal live imaging microscopy in plants," *Nat. Commun.* **12**, 1901 (2021).
124. Y. Zhang, *et al.*, "Nanoscale subcellular architecture revealed by multicolor three-dimensional salvaged fluorescence imaging," *Nat. Methods* **17**, 225 (2020).
125. R. Sikora *et al.*, "MICAL-L1 is required for cargo protein delivery to the cell surface," *Biol. Open* **10**, bio058008 (2021).
126. C. Herrera, N. J. Mantis, and R. Cole, "Applications in stimulated emission depletion microscopy: localization of a protein toxin in the endoplasmic reticulum following retrograde transport," *Microsc. Microanal.* **22**, 1113 (2016).
127. T. S. Kim *et al.*, "Molecular architecture of a cylindrical self-assembly at human centrosomes," *Nat. Commun.* **10**, 1151 (2019).
128. T. T. Yang *et al.*, "Super-resolution architecture of mammalian centriole distal appendages reveals distinct blade and matrix functional components," *Nat. Commun.* **9**, 2023 (2018).
129. A. M. Sydor *et al.*, "PPP1R35 is a novel centrosomal protein that regulates centriole length in concert with the microcephaly protein RTTN," *eLife* **7**, e37846 (2018).
130. M. Gao, "Expansion microscopy opens the door to exploring more challenges," *Nat. Methods* **12**, 147 (2022).
131. F. U. Zwettler *et al.*, "Molecular resolution imaging by post-labeling expansion single-molecule localization microscopy (Ex-SMLM)," *Nat. Commun.* **11**, 3388 (2020).

132. J. A. Ruland, *et al.*, "Nuclear export of the pre-60S ribosomal subunit through single nuclear pores observed in real time," *Nat. Commun.* **12**, 6211 (2021).
133. C. Deng *et al.*, "Impaired dynamic interaction of axonal endoplasmic reticulum and ribosomes contributes to defective stimulus-response in spinal muscular atrophy," *Trans. Neurodegener.* **11**, 31 (2022).
134. A. Maiser *et al.*, "Super-resolution *in situ* analysis of active ribosomal DNA chromatin organization in the nucleolus," *Sci. Rep.* **10**, 7462 (2020).
135. D. P. Hoffman *et al.*, "Correlative three-dimensional super-resolution and block-face electron microscopy of whole vitreously frozen cells," *Science* **367**, eaaz5357 (2020).
136. A. Klimas *et al.*, "Magnify is a universal molecular anchoring strategy for expansion microscopy," *Nat. Biotechnol.* **41**, 858 (2023).
137. M. H. Laporte *et al.*, "Visualizing the native cellular organization by coupling cryofixation with expansion microscopy (Cryo-ExM)," *Nat. Methods* **19**, 216 (2022).
138. S. C. M. Reinhardt *et al.*, "Ångström-resolution fluorescence microscopy," *Nature* **617**, 711 (2023).